Semi-implicit Interior Penalty Discontinuous Galerkin Methods for Viscous Compressible Flows

Vít Dolejší*

*Charles University Prague, Faculty of Mathematics and Physics,
Sokolovská 83, 186 75 Prague, Czech Republic*

Abstract. We deal with the numerical solution of the Navier-Stokes equations describing a motion of viscous compressible fluids. In order to obtain a sufficiently stable higher order scheme with respect to the time and space coordinates, we develop a combination of the discontinuous Galerkin finite element (DGFE) method for the space discretization and the backward difference formulae (BDF) for the time discretization. Since the resulting discrete problem leads to a system of nonlinear algebraic equations at each time step, we employ suitable linearizations of inviscid as well as viscous fluxes which give a linear algebraic problem at each time step. Finally, the resulting BDF-DGFE scheme is applied to steady as well as unsteady flows and achieved results are compared with reference data.

1 Introduction

Our aim is to develop a sufficiently robust, efficient and accurate numerical scheme for the simulation of unsteady compressible flows. In last years the *discontinuous Galerkin method* (DGM) was employed in many papers for the discretization of compressible fluid flow problems, see, e.g., [5], [6], [8], [10], [20], [32], [37], [38], [39], [40], [43], [44], [45], [56], [57] and the references cited therein. DGM is based on a piecewise polynomial but discontinuous approximation which provides robust and high-order accurate approximations, particularly in transport dominated regimes. Moreover, there is considerable flexibility in the choice of the mesh design; indeed, DGM can easily handle non-matching and non-uniform grids, even anisotropic, polynomial approximation degrees. This allows a simple treatment with *hp*-adaptation techniques. Additionally, orthogonal bases

---

*Corresponding author. *Email address:* `dolejsi@karlin.mff.cuni.cz`

can easily be constructed which lead to diagonal mass matrices; this is particularly advantageous for unsteady problems. Finally, in combination with block-type preconditioners, DGMs can easily be parallelized. For a survey about DGM, see [13] or [15].

There are several variants of the DGM for the solution of problems containing diffusion terms, see, e. g., [3]. It is possible to use a primal formulation or a mixed method. The method can be stabilized with the aid of a symmetric or non-symmetric treatment of diffusion terms, often combined with interior and boundary penalties. The mixed methods consider the gradient of the solution as an independent variable hence the second order derivative in the Navier-Stokes equations are eliminated and consequently, we obtain a problem with a higher number of unknowns, see, e.g., [6]. Nevertheless, an efficient implementation of mixed methods locally eliminates the auxiliary variables. A comparison of accuracy and robustness of the DGM based on the primal formulation from [10] and the mixed DGM from [6] was presented in [9].

Among methods using primal formulation, two approaches, *symmetric interior penalty Galerkin* (SIPG) and *non-symmetric interior penalty Galerkin* (NIPG) introduced in [2] and [50] are very popular, respectively. Moreover, we consider the so-called *incomplete interior penalty Galerkin* (IIPG) method which was studied in [17], [53], [54]. Although IIPG has not the favourable properties as NIPG and SIPG techniques (see Remark 4.3 of this paper), its application to the Navier-Stokes equations is more simple since some stabilization terms are missing. We analysed these techniques in [25], [27] (NIPG), [24], [26] (SIPG) and [22] (IIPG) for a scalar non-stationary convection-diffusion equation.

For unsteady problems, it is possible to use a discontinuous approximation also for the time discretization (e.g., [46], [56], [57]), but the most usual approach is an application of the method of lines. In this case, the Runge-Kutta methods are very popular for their simplicity and a high order of accuracy, see [6], [7], [8], [10], [14], [20], [38]. Their drawback is a strong restriction to the size of the time step. To avoid this disadvantage it is suitable to use an implicit time discretization, e.g., [39], [40]. However, a full implicit scheme leads to a necessity to solve a nonlinear system of algebraic equations at each time step which is rather expensive. Therefore, we proposed in [31] a semi-implicit method for the simulation of inviscid compressible flow. This technique is based on a suitable linearization of the Euler fluxes. The linear terms are treated implicitly whereas the nonlinear ones explicitly which leads to a linear algebraic problem at each time step.

In this paper, we extend the approach of semi-implicit scheme to the viscous case. Hence, this article is a natural combination of the explicit scheme for viscous flow from [20] with the semi-implicit scheme for inviscid flow from [31]. Moreover, we apply the *backward difference formula* (BDF) to the time discretization which gives a higher order approximation with respect to the time. This method was analysed in [29] for the case of a scalar non-stationary convection-diffusion equation.

The content of the rest of the paper is the following. In Section 2 we introduce the system of the compressible Navier-Stokes equations with appropriate initial and boundary conditions and mention some properties of inviscid and viscous fluxes. In Section 3 we discretize the computational domain and define spaces of discontinuous functions. In

Section 4 we recall the space discretization of a model scalar equation by the discontinuous Galerkin finite element method which was presented in former papers [22], [24], [25], [26], [27]. The novelty of this paper is contained in Section 5. We extend the discretization of the model problem to the system of Navier-Stokes equations, carry out the time discetization by a higher order semi-implicit scheme and mention several implementation remarks. Finally, three numerical examples, demonstrating the stability and accuracy of the method, are presented in Section 6. The concluding remarks are given in Section 7.

2 Problem formulation

2.1 Compressible flow problem

Let $\Omega \subset I\!R^d$, $d=2,3$ be a bounded domain and $T>0$. We set $Q_T = \Omega \times (0,T)$ and by $\partial \Omega$ denote the boundary of Ω which consists of several disjoint parts. We distinguish inlet $\partial \Omega_i$, outlet $\partial \Omega_o$ and impermeable walls $\partial \Omega_w$, i.e. $\partial \Omega = \partial \Omega_i \cup \partial \Omega_o \cup \partial \Omega_w$. The system of Navier-Stokes equations describing a motion of viscous compressible fluids can be written in the dimensionless form

$$\frac{\partial \boldsymbol{w}}{\partial t} + \nabla \cdot \vec{\boldsymbol{f}}(\boldsymbol{w}) = \nabla \cdot \vec{\boldsymbol{R}}(\boldsymbol{w}, \nabla \boldsymbol{w}) \quad \text{in } Q_T, \tag{2.1}$$

where

$$\boldsymbol{w} = (w_1, \dots, w_{d+2})^{\mathrm{T}} = (\rho, \rho v_1, \dots, \rho v_d, e)^{\mathrm{T}} \tag{2.2}$$

is the so-called *state vector*,

$$\vec{\boldsymbol{f}}(\boldsymbol{w}) = (\boldsymbol{f}_1(\boldsymbol{w}), \dots, \boldsymbol{f}_d(\boldsymbol{w})) \tag{2.3}$$

$$\text{with} \quad \boldsymbol{f}_s(\boldsymbol{w}) = (f_s^{(1)}(\boldsymbol{w}), \dots, f_s^{(d+2)}(\boldsymbol{w}))^{\mathrm{T}}$$

$$= (\rho v_s, \rho v_s v_1 + \delta_{s1} p, \dots, \rho v_s v_d + \delta_d p, (e+p)v_s)^{\mathrm{T}}, \quad s=1, \dots, d$$

are the so-called *inviscid (Euler) fluxes* and

$$\vec{\boldsymbol{R}}(\boldsymbol{w}) = (\boldsymbol{R}_1(\boldsymbol{w}), \dots, \boldsymbol{R}_d(\boldsymbol{w})) \tag{2.4}$$

$$\text{with} \quad \boldsymbol{R}_s(\boldsymbol{w}, \nabla \boldsymbol{w}) = (R_s^{(1)}(\boldsymbol{w}, \nabla \boldsymbol{w}), \dots, R_s^{(d+2)}(\boldsymbol{w}, \nabla \boldsymbol{w}))^{\mathrm{T}}$$

$$= \left(0, \tau_{s1}, \dots, \tau_{sd}, \sum_{k=1}^{d} \tau_{sk} v_k + \frac{\gamma}{Re\,Pr} \frac{\partial \theta}{\partial x_s} \right)^{\mathrm{T}}, \quad s=1, \dots, d$$

are the so-called *viscous fluxes*. Symbols ∇ and $\nabla \cdot$ mean the gradient and divergence operators, i.e.,

$$\nabla \boldsymbol{w} \equiv \left(\frac{\partial \boldsymbol{w}}{\partial x_1}, \dots, \frac{\partial \boldsymbol{w}}{\partial x_d} \right) \in I\!R^{d+2} \times \cdots \times I\!R^{d+2} \tag{2.5}$$

and

$$\nabla \cdot \vec{\boldsymbol{f}}(\boldsymbol{w}) \equiv \sum_{s=1}^{d} \frac{\partial \boldsymbol{f}_s(\boldsymbol{w})}{\partial x_s} \in I\!R^{d+2}, \tag{2.6}$$

respectively.

We consider the Newtonian type of fluid, i. e., the viscous part of the stress tensor has the form

$$\tau_{sk} = \frac{1}{Re}\left[\left(\frac{\partial v_s}{\partial x_k} + \frac{\partial v_k}{\partial x_s}\right) - \frac{2}{3}\sum_{i=1}^{d}\frac{\partial v_i}{\partial x_i}\delta_{sk}\right], \quad s,k=1,\ldots,d. \tag{2.7}$$

We use the following notation: ρ – density, p – pressure, e – total energy, $\boldsymbol{v} = (v_1,\ldots,v_d)$ – velocity, θ – temperature, γ – Poisson adiabatic constant, Re – Reynolds number, Pr – Prandtl number.

In order to close the system, we consider the state equation for perfect gas and the definition of the total energy

$$p = (\gamma-1)(e-\rho|\boldsymbol{v}|^2/2), \quad e = c_V\rho\theta + \rho|\boldsymbol{v}|^2/2, \tag{2.8}$$

where c_V is the specific heat at constant volume which we assume to be equal to one in the dimensionless case. The system (2.1) – (2.8) is of *hyperbolic-parabolic* type. It is equipped with the initial condition

$$\boldsymbol{w}(x,0) = \boldsymbol{w}^0(x), \quad x\in\Omega, \tag{2.9}$$

and the following set of boundary conditions on appropriate parts of boundary:

$$a) \quad \rho=\rho_D, \ \boldsymbol{v}=\boldsymbol{v}_D, \ \sum_{k=1}^{d}\left(\sum_{l=1}^{d}\tau_{lk}n_l\right)v_k + \frac{\gamma}{Re\,Pr}\frac{\partial\theta}{\partial\boldsymbol{n}}=0 \quad \text{on } \partial\Omega_i, \tag{2.10}$$

$$b) \quad \sum_{k=1}^{d}\tau_{sk}n_k=0, \ s=1,\ldots,d, \quad \frac{\partial\theta}{\partial\boldsymbol{n}}=0 \quad \text{on } \partial\Omega_o,$$

$$c) \quad \boldsymbol{v}=0, \frac{\partial\theta}{\partial\boldsymbol{n}}=0 \quad \text{on } \partial\Omega_w,$$

where ρ_D and $\boldsymbol{v}_D$ are given function and $\boldsymbol{n} = (n_1,\ldots,n_d)$ is a unit outer normal to $\partial\Omega$. Another possibility is to replace the adiabatic boundary condition (2.10), c) by

$$c') \ \boldsymbol{v}=0, \ \theta=\theta_D \quad \text{on } \partial\Omega_w. \tag{2.11}$$

In the case of vanishing viscosity (i.e., $Re\to\infty$), we obtain the reduced problem of the Euler equations. Thus the boundary conditions (2.10) should be replaced by the appropriate "inviscid conditions" which are chosen in such a way that the system of the Euler equations is linearly well-posed. Namely, for subsonic inlet we prescribe the density and components of velocity, for the subsonic outlet we prescribe the pressure and on solid walls the impermeability condition is used. For more details see, e.g., [35, Section 3.3.6].

The problem to solve the compressible Navier-Stokes equations (2.1) – (2.4) with constitutive relations (2.7) – (2.8), equipped with the initial and boundary conditions (2.9) – (2.11) will be denoted by (CFP) (compressible flow problem).

Finally, we present some properties of the inviscid and viscous fluxes $\vec{\boldsymbol{f}}(\cdot)$ and $\vec{\boldsymbol{R}}(\cdot,\cdot)$ given by (2.3) and (2.4), respectively. These properties are fundamental for introducing

the linearization of the nonlinear fluxes, which is the base of semi-implicit time discretization schemes.

The inviscid fluxes $\boldsymbol{f}_s$, $s=1,\ldots,d$ satisfy (see [35, Lemma 3.1])

$$\boldsymbol{f}_s(\boldsymbol{w}) = \boldsymbol{A}_s(\boldsymbol{w})\boldsymbol{w}, \quad s=1,\ldots,d, \tag{2.12}$$

where

$$\boldsymbol{A}_s(\boldsymbol{w}) \equiv \frac{D\boldsymbol{f}_s(\boldsymbol{w})}{D\boldsymbol{w}}, \quad s=1,\ldots,d, \tag{2.13}$$

are the Jacobi matrices of the mappings $\boldsymbol{f}_s$. Then, we define a matrix

$$\boldsymbol{P}(\boldsymbol{w},\boldsymbol{n}) \equiv \sum_{s=1}^{d} \boldsymbol{A}_s(\boldsymbol{w})n_s, \tag{2.14}$$

where $\boldsymbol{n}=(n_1,\ldots,n_d)\in I\!\!R^d$, $n_1^2+\cdots+n_d^2=1$, which plays a role in the definition of a numerical flux and the choice of boundary conditions.

Furthermore, the viscous terms $\boldsymbol{R}_s(\boldsymbol{w},\nabla\boldsymbol{w})$ can be expressed in the form

$$\boldsymbol{R}_s(\boldsymbol{w},\nabla\boldsymbol{w}) = \sum_{k=1}^{d} \boldsymbol{K}_{s,k}(\boldsymbol{w})\frac{\partial\boldsymbol{w}}{\partial x_k}, \quad s=1,\ldots,d, \tag{2.15}$$

where $\boldsymbol{K}_{s,k}(\cdot)$ are $(d+2)\times(d+2)$ matrices dependent on $\boldsymbol{w}$, see Appendix, expressions (7.1) – (7.6).

Moreover, in virtue of [20], we introduce another formal variant of the viscous terms. Let $\boldsymbol{w}=(w_1,\ldots,w_{d+2})\in I\!\!R^{d+2}$ and $\boldsymbol{\varphi}=(\varphi_1,\ldots,\varphi_{d+2})\in I\!\!R^{d+2}$ then putting $\nabla\boldsymbol{w}:=\nabla\boldsymbol{\varphi}$ in (2.15) we have

$$\boldsymbol{R}_s(\boldsymbol{w},\nabla\boldsymbol{\varphi}) = \sum_{k=1}^{d} \boldsymbol{K}_{s,k}(\boldsymbol{w})\frac{\partial\boldsymbol{\varphi}}{\partial x_k} \in I\!\!R^{d+2}, \quad s=1,\ldots,d. \tag{2.16}$$

The sum of the matrix-vector products (2.16) contains several terms

$$P\frac{w_j}{w_1}\frac{\partial\varphi_1}{\partial x_k}, \qquad j=2,\ldots,d+2, \quad k=1,\ldots,d, \tag{2.17}$$

where P symbolically denotes the rest of terms (P depends on $\boldsymbol{w}$). We replace these terms by

$$P\frac{\varphi_j}{w_1}\frac{\partial w_1}{\partial x_k}, \qquad j=2,\ldots,d+2, \quad k=1,\ldots,d \tag{2.18}$$

and then we obtain new functions

$$\boldsymbol{d}_s(\boldsymbol{w},\nabla\boldsymbol{w},\boldsymbol{\varphi},\nabla\boldsymbol{\varphi}) : I\!\!R^{d+2}\times I\!\!R^{d(d+2)}\times I\!\!R^{d+2}\times I\!\!R^{d(d+2)} \to I\!\!R^{d+2}, \, s=1,\ldots,d. \tag{2.19}$$

From the above construction it follows that $\boldsymbol{d}_s(\cdot,\cdot,\cdot,\cdot)$ are consistent with $\boldsymbol{R}_s(\cdot,\cdot)$ by

$$\boldsymbol{d}_s(\boldsymbol{w},\nabla\boldsymbol{w},\boldsymbol{w},\nabla\boldsymbol{w}) = \boldsymbol{R}_s(\boldsymbol{w},\nabla\boldsymbol{w}) \quad \forall\boldsymbol{w}, \, s=1,\ldots,d, \tag{2.20}$$

functions $\boldsymbol{d}_s(\boldsymbol{w}, \nabla\boldsymbol{w}, \boldsymbol{\varphi}, \nabla\boldsymbol{\varphi})$, $s = 1, \ldots, d$ are linear with respect to $\boldsymbol{\varphi}$ and they are independent of $\nabla\varphi_1$.

The functions $\boldsymbol{d}_s$, $s = 1, \ldots, d$ can be written as a sum of matrix-vector products by

$$\boldsymbol{d}_s(\boldsymbol{w}, \nabla\boldsymbol{w}, \boldsymbol{\varphi}, \nabla\boldsymbol{\varphi}) \equiv \boldsymbol{D}_{s,0}(\boldsymbol{w}, \nabla\boldsymbol{w})\boldsymbol{\varphi} + \sum_{k=1}^{d} \boldsymbol{D}_{s,k}(\boldsymbol{w})\frac{\partial\boldsymbol{\varphi}}{\partial x_k}, \quad s = 1, \ldots, d, \tag{2.21}$$

where $\boldsymbol{D}_{s,k}$, $k = 0, 1, \ldots, d$, $s = 1, \ldots, d$ are $(d+2) \times (d+2)$ matrices, see Appendix, expressions (7.7) – (7.10).

3 Discretization

3.1 Triangulations

Let $\mathcal{T}_h$ ($h > 0$) be a partition of the domain Ω into a finite number of closed d-dimensional mutually disjoint (convex or non-convex) polyhedra K i.e., $\overline{\Omega} = \bigcup_{K \in \mathcal{T}_h} K$. We call $\mathcal{T}_h = \{K\}_{K \in \mathcal{T}_h}$ a *triangulation* of Ω and do not require the conforming properties from the finite element method, see [12], [55]. In 2D problems, we choose usually $K \in \mathcal{T}_h$ as triangles or quadrilaterals. In 3D, $K \in \mathcal{T}_h$ can be, e. g., tetrahedra, pyramids or hexahedra, but we can construct even more general elements K, as dual finite volumes from [34]. By ∂K we denote the boundary of element $K \in \mathcal{T}_h$ and set $h_K = \mathrm{diam}(K)$, $h = \max_{K \in \mathcal{T}_h} h_K$. By ρ_K we denote the radius of the largest d-dimensional ball inscribed into K and by $|K|$ we denote the d-dimensional Lebesgue measure of K.

By $\mathcal{F}_h$ we denote the smallest possible set of all open $(d-1)$-dimensional faces (open edges when $d = 2$ or open faces when $d = 3$) of all elements $K \in \mathcal{T}_h$, see Figure 1. Further, we denote by $\mathcal{F}_h^I$ the set of all $\Gamma \in \mathcal{F}_h$ that are contained in Ω (inner faces). Moreover, we denote by $\mathcal{F}_h^w$, $\mathcal{F}_h^i$ and $\mathcal{F}_h^o$ the set of all $\Gamma \in \mathcal{F}_h$ such that $\Gamma \subset \partial\Omega_w$, $\Gamma \subset \partial\Omega_i$ and $\Gamma \subset \partial\Omega_o$, respectively. Furthermore, we denote by $\mathcal{F}_h^D$ the set of all $\Gamma \in \mathcal{F}_h$ where the Dirichlet type of boundary conditions is prescribed at least for one component of $\boldsymbol{w}$ (i.e., $\mathcal{F}_h^D \equiv \mathcal{F}_h^w \cup \mathcal{F}_h^i$) and by $\mathcal{F}_h^N$ the set of all $\Gamma \in \mathcal{F}_h$ where the Neumann type of boundary conditions is prescribed for all components of $\boldsymbol{w}$ (i.e., $\mathcal{F}_h^N \equiv \mathcal{F}_h^o$). Obviously, $\mathcal{F}_h = \mathcal{F}_h^I \cup \mathcal{F}_h^D \cup \mathcal{F}_h^N$. For a shorter notation we put $\mathcal{F}_h^{io} \equiv \mathcal{F}_h^i \cup \mathcal{F}_h^o$, $\mathcal{F}_h^{ID} \equiv \mathcal{F}_h^I \cup \mathcal{F}_h^D$ and $\mathcal{F}_h^{DN} \equiv \mathcal{F}_h^D \cup \mathcal{F}_h^N = \mathcal{F}_h^w \cup \mathcal{F}_h^i \cup \mathcal{F}_h^o$.

Finally, for each $\Gamma \in \mathcal{F}_h$ we define a unit normal vector $\boldsymbol{n}_\Gamma$. We assume that $\boldsymbol{n}_\Gamma$, $\Gamma \in \mathcal{F}_h^{DN}$ has the same orientation as the outer normal of $\partial\Omega$. For $\boldsymbol{n}_\Gamma$, $\Gamma \in \mathcal{F}_h^I$ the orientation is arbitrary but fixed for each edge, see Figure 1.

Remark 3.1. DGM is capable to treat concave elements as it is shown in Figure 1. There is a question if the use of such elements does not decrease the order of accuracy of the method. Numerical analysis carried out in [27] for a scalar nonlinear convection-diffusion equation gives the same error estimate for convex as well as non-convex elements. Moreover, numerical experiments carried out in [25] for the same scalar equation
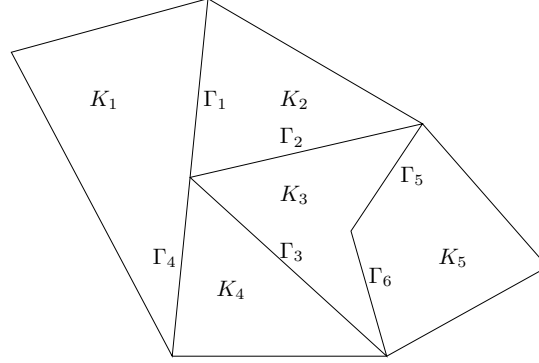
Figure 1: Example of elements K_l, $l=1,\ldots,5$ and faces Γ_l, $l=1,\ldots,6$ with the corresponding $\boldsymbol{n}_{\Gamma_l}$

give the second order of convergence in the L^2-norm for the piecewise linear approximation. However, the use of concave elements for the Navier-Stokes equations was not tested yet.

3.2 Discontinuous finite element spaces

To each $K \in \mathcal{T}_h$, we assign a positive integer s_K (local Sobolev index) and a positive integer p_K (local polynomial degree) . Then we define the vectors

$$\mathsf{s} \equiv \{s_K, K \in \mathcal{T}_h\}, \qquad \mathsf{p} \equiv \{p_K, K \in \mathcal{T}_h\}. \tag{3.1}$$

Over the triangulation $\mathcal{T}_h$ we define the so-called *broken Sobolev space* corresponding to the vector s

$$H^{\mathsf{s}}(\Omega, \mathcal{T}_h) \equiv \{v; v|_K \in H^{s_K}(K) \ \forall K \in \mathcal{T}_h\}. \tag{3.2}$$

If $s_K = q \ \forall K \in \mathcal{T}_h$, $q \in I\!N$ then we use the notation $H^q(\Omega, \mathcal{T}_h) = H^{\mathsf{s}}(\Omega, \mathcal{T}_h)$. Obviously,

$$H^{\bar{s}}(\Omega, \mathcal{T}_h) \subset H^{\mathsf{s}}(\Omega, \mathcal{T}_h) \subset H^{\underline{\mathsf{s}}}(\Omega, \mathcal{T}_h), \tag{3.3}$$

where $\bar{s} = \max\{s_K, s_K \in \mathsf{s}\}$ and $\underline{s} = \min\{s_K, s_K \in \mathsf{s}\}$.

Furthermore, we define the space of discontinuous piecewise polynomial functions associated with the vector p by

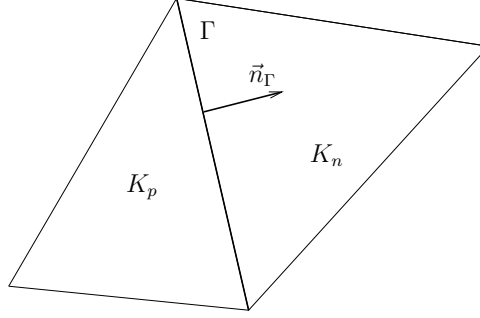$$S_{h\mathsf{p}} \equiv \{v; \ v \in L^2(\Omega), \ v|_K \in P_{p_K}(K) \ \forall K \in \mathcal{T}_h\}, \tag{3.4}$$

Figure 2: Inner edge Γ, elements K_p and K_n and the orientation of $\boldsymbol{n}_\Gamma$

where $P_{p_K}(K)$ denotes the space of all polynomials on K of degree $\leq p_K$, $K \in \mathcal{T}_h$. We seek the approximate solution in the space of vector-valued functions

$$\boldsymbol{S}_{h\mathbf{p}} \equiv \underbrace{S_{h\mathbf{p}} \times \cdots \times S_{h\mathbf{p}}}_{d+2 \text{ times}}. \tag{3.5}$$

For each $\Gamma \in \mathcal{F}_h^I$ there exist two elements $K_p, K_n \in \mathcal{T}_h$ such that $\Gamma \subset K_p \cap K_n$. We use a convention that K_n lies in the direction of $\boldsymbol{n}_\Gamma$ and K_p in the opposite direction of $\boldsymbol{n}_\Gamma$, see Figure 2. Then for $v \in H^1(\Omega, \mathcal{T}_h)$, we introduce the notation:

$$\begin{aligned}
v|_\Gamma^{(p)} &\equiv \text{ the trace of } v|_{K_p} \text{ on } \Gamma, \tag{3.6}\\
v|_\Gamma^{(n)} &\equiv \text{ the trace of } v|_{K_n} \text{ on } \Gamma, \\
\langle v \rangle_\Gamma &\equiv \frac{1}{2}\left(v|_\Gamma^{(p)} + v|_\Gamma^{(n)}\right), \\
[v]_\Gamma &\equiv v|_\Gamma^{(p)} - v|_\Gamma^{(n)}.
\end{aligned}$$

The value $[v]_\Gamma$ depends on the orientation of $\boldsymbol{n}_\Gamma$ of course but the value $[v]_\Gamma \boldsymbol{n}_\Gamma$ does not. Further, we put

$$d(\Gamma) \equiv \min(h_{K_p}, h_{K_n}), \quad \Gamma \in \mathcal{F}_h^I. \tag{3.7}$$

For $\Gamma \in \mathcal{F}_h^{DN}$ there exists element $K_p \in \mathcal{T}_h$ such that $\Gamma \subset K_p \cap \partial\Omega$. Then for $v \in H^1(\Omega, \mathcal{T}_h)$, we introduce the notation:

$$\begin{aligned}
v|_\Gamma^{(p)} &\equiv \text{ the trace of } v|_{K_p} \text{ on } \Gamma, \tag{3.8}\\
\langle v \rangle_\Gamma &\equiv [v]_\Gamma \equiv v|_\Gamma^{(p)}.
\end{aligned}$$

By $v|_\Gamma^{(n)}$, $\Gamma \in \mathcal{F}_h^D \cup \mathcal{F}_h^N$ we formally denote the trace of v on Γ from the exterior of Ω given either by a boundary condition or by an extrapolation from the interior of Ω. Additionally, we associate with the face $\Gamma \in \mathcal{F}_h^{DN}$ the unit normal vector $\boldsymbol{n} = \boldsymbol{n}_\Gamma$ which points from

K_p to the exterior of Ω. In virtue of (3.7), we put

$$d(\Gamma) \equiv h_{K_p}, \quad \Gamma \in \mathcal{F}_h^{DN}. \tag{3.9}$$

In case that $[\cdot]_\Gamma$ and $\langle\cdot\rangle_\Gamma$ are arguments of $\int_\Gamma \ldots dS$, $\Gamma \in \mathcal{F}_h$ we omit the subscript Γ and write simply $[\cdot]$ and $\langle\cdot\rangle$, respectively.

4   Model scalar equation

We start with the DGFE solution of the following model non-stationary scalar convection-diffusion equation. We seek $u : Q_T = \Omega \times (0,T) \to I\!R$ such that

$$
\begin{align}
\text{a)} \quad & \frac{\partial u}{\partial t} + \nabla \cdot \vec{f}(u) = \varepsilon \Delta u \quad \text{in } Q_T, \notag \\
\text{b)} \quad & u\big|_{\partial\Omega_D \times (0,T)} = u_D, \notag \\
\text{c)} \quad & \frac{\partial u}{\partial \boldsymbol{n}}\Big|_{\partial\Omega_N \times (0,T)} = g_N, \notag \\
\text{d)} \quad & u(x,0) = u^0(x), \quad x \in \Omega, \notag
\end{align}
\tag{4.1}
$$

where $\varepsilon > 0$ plays a role of viscosity, $u_D : \partial\Omega_D \times (0,T) \to I\!R$, $g_N : \partial\Omega_N \times (0,T) \to I\!R$ and $u^0 : \Omega \to I\!R$ are given functions, $\boldsymbol{n} = (n_1,\ldots,n_d)$ is a unit outer normal to $\partial\Omega$, and $\vec{f} = (f_1,\ldots,f_d) : I\!R \to I\!R^d$ are prescribed continuous functions representing convection fluxes.

The interior penalty approach for the DGFE discretization of (4.1) can be found in many papers, e.g., [3], [4], [20], [27], [42], [49], [51] and the references therein. Hence, we do not derive it again and present only the final expressions.

We multiply (4.1) by a function $v \in H^2(\Omega, \mathcal{T}_h)$, integrate over $K \in \mathcal{T}_h$, use the Green's theorem, sum over $K \in \mathcal{T}_h$ and add the penalty terms vanishing for a continuous solution u. Then the *discontinuous Galerkin finite element* (DGFE) formulation of (4.1) reads

$$\left(\frac{\partial u}{\partial t}, v\right) + a_h(u,v) + \tilde{b}_h(u,v) + J_h^\sigma(u,v) = \ell_h(v), \tag{4.2}$$

where

$$a_h(u,v) = \varepsilon \sum_{K \in \mathcal{T}_h} \int_K \nabla u \cdot \nabla v\, dx - \varepsilon \sum_{\Gamma \in \mathcal{F}_h^{ID}} \int_\Gamma (\langle \nabla u \cdot \boldsymbol{n}\rangle [v] + \eta \langle \nabla v \cdot \boldsymbol{n}\rangle [u])\, dS, \tag{4.3}$$

$$J_h^\sigma(u,v) = \sum_{\Gamma \in \mathcal{F}_h^{ID}} \int_\Gamma \sigma [u][v]\, dS, \tag{4.4}$$

$$\ell_h(v)(t) = \sum_{\Gamma \in \mathcal{F}_h^N} \int_\Gamma g_N(t) v\, dS - \varepsilon\eta \sum_{\Gamma \in \mathcal{F}_h^D} \int_\Gamma \nabla v \cdot \boldsymbol{n} u_D(t)\, dS + \sum_{\Gamma \in \mathcal{F}_h^D} \int_\Gamma \sigma u_D(t) v\, dS, \tag{4.5}$$

$$\tilde{b}_h(u,v) = -\sum_{K \in \mathcal{T}_h} \int_K \vec{f}(u) \cdot \nabla v\, dx + \sum_{K \in \mathcal{T}_h} \int_{\partial K} \vec{f}(u) \cdot \boldsymbol{n}_{\partial K} v\, dS, \tag{4.6}$$

where $\boldsymbol{n}_{\partial K}$ is the unit outer normal to $K \in \mathcal{T}_h$ on ∂K, $\eta \in I\!R$ is a parameter (see Remark 4.3) and the penalty parameter σ in (4.4) and (4.5) is defined by

$$\sigma|_\Gamma = \varepsilon \frac{C_W}{d(\Gamma)}, \quad \Gamma \in \mathcal{F}_h^{ID}, \tag{4.7}$$

where $d(\Gamma)$ is given either by (3.7) or (3.9) and $C_W > 0$ is a suitable constant.

Remark 4.1. The first two terms in (4.3),

$$\varepsilon \sum_{K \in \mathcal{T}_h} \int_K \nabla u \cdot \nabla v \, \mathrm{d}x \quad \text{and} \quad -\varepsilon \sum_{\Gamma \in \mathcal{F}_h^{ID}} \int_\Gamma \langle \nabla u \cdot \boldsymbol{n} \rangle [v] \, \mathrm{d}S, \tag{4.8}$$

arise from the multiplication of the diffusive term $-\varepsilon \Delta u$ by $v \in H^2(\Omega, \mathcal{T}_h)$, the use of Green's theorem and the sum over $K \in \mathcal{T}_h$. Moreover, in the definition of the *diffusion form* $a_h(\cdot, \cdot)$ given by (4.3), we add integrals

$$-\varepsilon \eta \sum_{\Gamma \in \mathcal{F}_h^{ID}} \int_\Gamma \langle \nabla v \cdot \boldsymbol{n} \rangle [u] \, \mathrm{d}S, \tag{4.9}$$

which follow from a formal exchange of u and v in the second term of (4.8). This term ensures the stability properties of the DGFE method, see the cited references above.

Remark 4.2. The form $J_h^\sigma(\cdot, \cdot)$ given by (4.4) represents the *interior and boundary penalty terms*. It guarantees (in some weaker sense) the interelement continuity of discontinuous approximation. If $u \in H^2(\Omega)$ is the solution of (4.2) satisfying the Dirichlet boundary condition (4.1), b) then $[u]_\Gamma = 0$, $\Gamma \in \mathcal{F}_h^I$ since u is continuous across interior faces. Consequently, it is easy to observe that the integrals (4.9) are compensated by the second term in the form $\ell_h(\cdot)$ (representing the treatment of boundary conditions) since

$$-\varepsilon \eta \sum_{\Gamma \in \mathcal{F}_h^{ID}} \int_\Gamma \langle \nabla v \cdot \boldsymbol{n} \rangle [u] \, \mathrm{d}S = \underbrace{-\varepsilon \sum_{\Gamma \in \mathcal{F}_h^I} \int_\Gamma \eta \langle \nabla v \cdot \boldsymbol{n} \rangle [u] \, \mathrm{d}S}_{=0} - \varepsilon \sum_{\Gamma \in \mathcal{F}_h^D} \int_\Gamma \eta \langle \nabla v \cdot \boldsymbol{n} \rangle [u] \, \mathrm{d}S$$

$$= -\varepsilon \eta \sum_{\Gamma \in \mathcal{F}_h^D} \int_\Gamma \nabla v \cdot \boldsymbol{n} u_D(t) \, \mathrm{d}S. \tag{4.10}$$

Moreover, the interior and boundary penalty terms are compensated by the third term of $\ell_h(\cdot)$ since

$$\sum_{\Gamma \in \mathcal{F}_h^{ID}} \int_\Gamma \sigma [u][v] \, \mathrm{d}S = \underbrace{\sum_{\Gamma \in \mathcal{F}_h^I} \int_\Gamma \sigma [u][v] \, \mathrm{d}S}_{=0} + \sum_{\Gamma \in \mathcal{F}_h^D} \int_\Gamma \sigma [u][v] \, \mathrm{d}S = \sum_{\Gamma \in \mathcal{F}_h^D} \int_\Gamma \sigma u_D(t) v. \tag{4.11}$$

The identities (4.10) and (4.11) imply the consistency of the DGFE formulation (4.2) with the weak formulation of (4.1).

Remark 4.3. The value of η appearing in (4.3) and (4.5) can be chosen arbitrarily but the most usual are the values $-1, 0$ and 1. Then we obtain three variants of the DGFE scheme:

- $\eta = 1$ – *symmetric interior penalty Galerkin* (SIPG) [2] which leads to a symmetric form $a_h(\cdot, \cdot) + J_h^\sigma(\cdot, \cdot)$. Consequently, it is possible to derive optimal a priori error estimates in the L^2-norm using the Aubin-Nitsch theorem provided that C_W in (4.7) is sufficiently large.

- $\eta = -1$ – *non-symmetric interior penalty Galerkin* (NIPG) [49], [50] which does not give optimal order of convergence in the L^2-norm but on the other hand, leads to a coercive form $a_h(\cdot, \cdot) + J_h^\sigma(\cdot, \cdot)$ for any $C_W > 0$ in (4.7). This is a favourable property, namely for an extension of the DGFE method to (CFP) where a numerical analysis is almost impossible and it is not clear how large C_W in (4.7) should be chosen.

- $\eta = 0$ – *incomplete interior penalty Galerkin* (IIPG) [17], [53], [54] which does not give optimal order of convergence in the L^2-norm and $C_W > 0$ in (4.7) should be chosen sufficiently large in order to guarantee the coercivity of form $a_h(\cdot, \cdot) + J_h^\sigma(\cdot, \cdot)$. However, IIPG formulation is more simple for implementation since integrals of type (4.9) appearing in (4.3) and (4.5) are missing. Moreover, this technique is more suitable for problems with nonlinear diffusion, see [22].

Remark 4.4. The integrand of the face integral (4.6) is approximated by the so-called *numerical flux* well-known from the finite volume method (see, e.g., [35, Section 3.2] or [60]) by

$$\vec{f}(u) \cdot \boldsymbol{n}_{\partial K} v \Big|_{\partial K} \approx H\left(u|_{\Gamma}^{(\mathrm{in})}, u|_{\Gamma}^{(\mathrm{out})}, \boldsymbol{n}_{\partial K} \right) v \Big|_{\partial K}, \tag{4.12}$$

where $u|_{\Gamma}^{(\mathrm{in})}$, $u|_{\Gamma}^{(\mathrm{out})}$ are the traces of u on ∂K from the interior and the exterior of element $K \in \mathcal{T}_h$, respectively. We assume standard properties of the numerical flux, namely consistency, conservativity and the Lipschitz continuity, see, e.g., [35]. Then we define the *discrete convective form*

$$b_h(u, v) = -\sum_{K \in \mathcal{T}_h} \int_K \vec{f}(u) \cdot \nabla v \, \mathrm{d}x + \sum_{\Gamma \in \mathcal{F}_h} \int_\Gamma H\left(u|_{\Gamma}^{(p)}, u|_{\Gamma}^{(n)}, \boldsymbol{n}_\Gamma \right) [v]_\Gamma \, \mathrm{d}S, \tag{4.13}$$

where $u|_{\Gamma}^{(p)}$ and $u|_{\Gamma}^{(n)}$ are given by (3.6). The form $b_h(u, v)$ is consistent with $\tilde{b}_h(\cdot, \cdot)$ by

$$b_h(u, v) = \tilde{b}_h(u, v) \quad \forall u \in H^2(\Omega), \, \forall v \in H^1(\Omega, \mathcal{T}_h). \tag{4.14}$$

Now we can introduce the *semi-discrete problem* of the model scalar equation (4.1):

Definition 4.1. Let $u_h^0 \in S_{h\mathrm{p}}$ be the $L^2(\Omega)$-projection of the initial condition u^0 into $S_{h\mathrm{p}}$, i.e. a function defined by

$$(u_h^0 - u^0, v_h) = 0 \quad \forall v_h \in S_{h\mathrm{p}}. \tag{4.15}$$

We say that u_h is a DGFE solution of (4.1), if

a) $u_h \in C^1(0,T;S_{h\mathbf{p}})$,

b) $\left(\dfrac{\partial u_h(t)}{\partial t},v_h\right)+b_h(u_h(t),v_h)+a_h(u_h(t),v_h)+J_h^\sigma(u_h(t),v_h)=\ell_h(v_h)(t)$

$$\forall v_h \in S_{h\mathbf{p}}, \ \forall t \in (0,T),$$ (4.16)

c) $u_h(0)=u_h^0$,

where $C^1(0,T;S_{h\mathbf{p}})$ is the space of continuously differentiable mappings of the interval $(0,T)$ into $S_{h\mathbf{p}}$.

The numerical scheme (4.16) represents a system of ordinary differential equations (ODEs) which should be solved by a suitable solver. We analysed this scheme in several papers ([22], [24], [25], [26], [27]) where a priori error estimates and numerical verification of theoretical results are presented. In the following section, we apply the DGFE scheme of type (4.16) to (CFP) introduced in Section 2.

5 System of the Navier-Stokes equations

Within this section, we extend the discontinuous Galerkin finite element method to the system of the compressible Navier-Stokes equations. First, we carried out the DGFE formulation of system (2.1) similarly as in (4.2) and consequently, we define the space discretization of (2.1). Furthermore, we deal with the time discretization of the resulting system of ODEs. Finally, we mention some implementation aspects.

5.1 DGFE formulation

The crucial item of the DGFE formulation of (CFP) is the treatment of the viscous terms. Let $w \in H^2(\Omega)^{d+2}$, then multiplying the viscous term $\nabla \cdot \vec{R}(w,\nabla w)$ from (2.1) by $\varphi \in H^2(\Omega,\mathcal{T}_h)^{d+2}$, integrating over $K \in \mathcal{T}_h$, summing over all $K \in \mathcal{T}_h$ and using (2.10), b) and (2.15), we obtain

$$-\sum_{K\in\mathcal{T}_h}\int_K\sum_{s=1}^d R_s(w,\nabla w)\cdot\frac{\partial\varphi}{\partial x_s}\mathrm{d}x+\sum_{\Gamma\in\mathcal{F}_h^{ID}}\int_\Gamma\sum_{s=1}^d\langle R_s(w,\nabla w)\rangle n_s\cdot[\varphi]\mathrm{d}S \qquad (5.1)$$

$$=\ -\sum_{K\in\mathcal{T}_h}\int_K\sum_{s=1}^d R_s(w,\nabla w)\cdot\frac{\partial\varphi}{\partial x_s}\mathrm{d}x+\sum_{\Gamma\in\mathcal{F}_h^{ID}}\int_\Gamma\sum_{s=1}^d\left\langle\sum_{k=1}^d K_{s,k}(w)\frac{\partial w}{\partial x_k}\right\rangle n_s\cdot[\varphi]\mathrm{d}S.$$

In virtue of Remark 4.1 we add to this expression a *stabilization term* which we obtain by the formal exchange of arguments w and φ in the last term of (5.1), i.e.,

$$\eta\sum_{\Gamma\in\mathcal{F}_h^{ID}}\int_\Gamma\sum_{s=1}^d\left\langle\sum_{k=1}^d K_{s,k}(w)\frac{\partial\varphi}{\partial x_k}\right\rangle n_s\cdot[w]\mathrm{d}S, \qquad (5.2)$$

where $\eta = -1,1$ depending on the type of stabilization, i.e., NIPG or SIPG variants. However, numerical experiments indicate that this choice of stabilization is not suitable. It is caused by that fact that for $\boldsymbol{\varphi} = (\varphi_1, 0, \ldots, 0)^{\mathrm{T}}$, $\varphi_1 \in H^2(\Omega, \mathcal{T}_h)$, $\varphi_1 \neq const$, we obtain a non-vanishing term (5.2) whereas both terms in (5.1) are equal to zero since the first rows of R_s, $K_{s,k}$, $s, k = 1, \ldots, d$ vanish, see (2.4) and (7.1) – (7.6). Therefore, in [10], [39], [40], the stabilization term

$$\eta \sum_{\Gamma \in \mathcal{F}_h^{ID}} \int_\Gamma \sum_{s=1}^d \left\langle \sum_{k=1}^d K_{s,k}^{\mathrm{T}}(\boldsymbol{w}) \frac{\partial \boldsymbol{\varphi}}{\partial x_k} \right\rangle n_s \cdot [\boldsymbol{w}] \mathrm{d}S. \tag{5.3}$$

was employed which avoids the drawback mentioned above. Here, K^{T} denotes the matrix transposed to K.

Moreover, in [20], we developed a different approach when the stabilization terms are treated as

$$\eta \sum_{\Gamma \in \mathcal{F}_h^{ID}} \int_\Gamma \sum_{s=1}^d \left\langle d_s(\boldsymbol{w}, \nabla \boldsymbol{w}, \boldsymbol{\varphi}, \nabla \boldsymbol{\varphi}) \right\rangle n_s \cdot [\boldsymbol{w}] \mathrm{d}S \tag{5.4}$$

$$= \eta \sum_{\Gamma \in \mathcal{F}_h^{ID}} \int_\Gamma \sum_{s=1}^d \left\langle D_{s,0}(\boldsymbol{w}, \nabla \boldsymbol{w}) \boldsymbol{\varphi} + \sum_{k=1}^d D_{s,k}(\boldsymbol{w}) \frac{\partial \boldsymbol{\varphi}}{\partial x_k} \right\rangle n_s \cdot [\boldsymbol{w}] \mathrm{d}S,$$

where $d_s(\cdot, \cdot, \cdot, \cdot)$, $s = 1, \ldots, d$ is given by (2.21) and $D_{s,k}$, $k = 0, 1, \ldots, d$, $s = 1, \ldots, d$ by (7.7) – (7.10). The forms $d_s(\cdot, \cdot, \cdot, \cdot)$, $s = 1, \ldots, d$ are linear with respect to their third and fourth arguments and integrals (5.4) vanish for $\boldsymbol{\varphi} = (\varphi_1, 0, \ldots, 0)^{\mathrm{T}} \in I\!\!R^{d+2}$, $\varphi_1 \in H^2(\Omega, \mathcal{T}_h)$ since d_s, $s = 1, \ldots, d$ are independent of $\nabla \varphi_1$ (see the construction of d_s, $s = 1, \ldots, d$ by (2.16) – (2.19)).

In order to simplify the notation we put

$$\boldsymbol{Q}_s(\boldsymbol{w}, \nabla \boldsymbol{w}, \boldsymbol{\varphi}, \nabla \boldsymbol{\varphi}) \equiv \begin{cases} \sum_{k=1}^d K_{s,k}^{\mathrm{T}}(\boldsymbol{w}) \frac{\partial \boldsymbol{\varphi}}{\partial x_k} & \text{for stabilization (5.3)} \\ d_s(\boldsymbol{w}, \nabla \boldsymbol{w}, \boldsymbol{\varphi}, \nabla \boldsymbol{\varphi}) & \text{for stabilization (5.4)} \end{cases}, \quad s = 1, \ldots, d. \tag{5.5}$$

Therefore, in virtue of the DGFE formulation carried out for the model problem in Section 4, we define for $\boldsymbol{w}, \boldsymbol{\varphi} \in H^2(\Omega, \mathcal{T}_h)^{d+2}$ the forms

$$(\boldsymbol{w}, \boldsymbol{\varphi}) = \sum_{K \in \mathcal{T}_h} \int_K \boldsymbol{w} \cdot \boldsymbol{\varphi} \mathrm{d}x \tag{5.6}$$

(L^2-scalar product),

$$\tilde{a}_h(\boldsymbol{w},\boldsymbol{\varphi}) \;=\; \sum_{K\in\mathcal{T}_h}\int_K \vec{R}(\boldsymbol{w},\nabla\boldsymbol{w})\cdot\nabla\boldsymbol{\varphi}\,\mathrm{d}x \tag{5.7}$$

$$- \sum_{\Gamma\in\mathcal{F}_h^{ID}}\int_\Gamma \sum_{s=1}^d \left\langle \sum_{k=1}^d K_{s,k}(\boldsymbol{w})\frac{\partial\boldsymbol{w}}{\partial x_k}\right\rangle n_s\cdot[\boldsymbol{\varphi}]\,\mathrm{d}S$$

$$-\eta \sum_{\Gamma\in\mathcal{F}_h^{ID}}\int_\Gamma \sum_{s=1}^d \langle Q_s(\boldsymbol{w},\nabla\boldsymbol{w},\boldsymbol{\varphi},\nabla\boldsymbol{\varphi})\rangle n_s\cdot[\boldsymbol{w}]\,\mathrm{d}S$$

$$+\eta \sum_{\Gamma\in\mathcal{F}_h^{D}}\int_\Gamma \sum_{s=1}^d Q_s(\boldsymbol{w},\nabla\boldsymbol{w},\boldsymbol{\varphi},\nabla\boldsymbol{\varphi})n_s\cdot\boldsymbol{w}_B\,\mathrm{d}S$$

(diffusion form),

$$\tilde{b}_h(\boldsymbol{w},\boldsymbol{\varphi})= \sum_{K\in\mathcal{T}_h}\left\{\int_{\partial K}\sum_{s=1}^d f_s(\boldsymbol{w})n_s\cdot\boldsymbol{\varphi}\,\mathrm{d}S - \int_K \sum_{s=1}^d f(\boldsymbol{w})\cdot\frac{\partial\boldsymbol{\varphi}}{\partial x_s}\,\mathrm{d}x\right\} \tag{5.8}$$

(convective form),

$$J_h^\sigma(\boldsymbol{w},\boldsymbol{\varphi})= \sum_{\Gamma\in\mathcal{F}_h^{ID}}\int_\Gamma \sigma[\boldsymbol{w}]\cdot[\boldsymbol{\varphi}]\,\mathrm{d}S - \sum_{\Gamma\in\mathcal{F}_h^{D}}\int_\Gamma \sigma\boldsymbol{w}_B\cdot\boldsymbol{\varphi}\,\mathrm{d}S \tag{5.9}$$

(interior and boundary penalty terms), where the penalty parameter σ is chosen by

$$\sigma|_\Gamma = \frac{C_W}{d(\Gamma)\,Re}, \quad \Gamma\in\mathcal{F}_h^{ID}, \tag{5.10}$$

where $d(\Gamma)$ is given either by (3.7) or (3.9) and $C_W>0$ is a suitable constant. The state vector $\boldsymbol{w}_B$ prescribed on $\partial\Omega_i\cup\partial\Omega_w$ is given by the boundary conditions, in particular, for the case (2.10) a)–c) we have

$$\boldsymbol{w}_B \;=\; (\rho|_{\partial\Omega_w},0,\ldots,0,\rho|_{\partial\Omega_w}\theta|_{\partial\Omega_w}) \text{ on } \partial\Omega_w, \tag{5.11}$$

$$\boldsymbol{w}_B \;=\; (\rho_D,\rho_D(\boldsymbol{v}_D)_1,\ldots,\rho_D(\boldsymbol{v}_D)_d,\rho|_{\partial\Omega_i}\theta|_{\partial\Omega_i}+\frac{1}{2}\rho_D|\boldsymbol{v}_D|^2) \text{ on } \partial\Omega_i,$$

and for the case (2.10) a)–b), (2.11) c′)

$$\boldsymbol{w}_B \;=\; (\rho|_{\partial\Omega_w},0,\ldots,0,\rho|_{\partial\Omega_w}\theta_D) \text{ on } \partial\Omega_w, \tag{5.12}$$

$$\boldsymbol{w}_B \;=\; (\rho_D,\rho_D(\boldsymbol{v}_D)_1,\ldots,\rho_D(\boldsymbol{v}_D)_d,\rho|_{\partial\Omega_i}\theta|_{\partial\Omega_i}+\frac{1}{2}\rho_D|\boldsymbol{v}_D|^2) \text{ on } \partial\Omega_i,$$

where $\rho_D,\boldsymbol{v}_D$ and θ_D are given functions from the boundary conditions (2.10)–(2.11) and $\rho|_\Gamma$ and $\theta|_\Gamma$ are the values of density and temperature extrapolated from interior of Ω on

the appropriate boundary part, respectively. More detailed determination of (5.7) – (5.12) is given in [20].

Let $w(t)$ denotes the function on Ω such that $w(t)(x) = w(x,t)$, $x \in \Omega$. Then with the aid of (5.6) – (5.9) the DGFE formulation for the Navier-Stokes equations reads

$$\frac{\mathrm{d}}{\mathrm{d}t}(w(t),\varphi) + \tilde{a}_h(w(t),\varphi) + \tilde{b}_h(w(t),\varphi) + J_h^\sigma(w(t),\varphi) = 0, \tag{5.13}$$

$$w(t),\varphi \in H^2(\Omega,\mathcal{T}_h)^{d+2}, \ t \in (0,T).$$

5.2 Space discretization

Within this section we deal with the space discretization of (5.13). In order to evaluate the boundary integrals in (5.8) we use the ("finite volume") approximation

$$\sum_{s=1}^{d} f_s(w)(n_{\partial K})_s \cdot \varphi \bigg|_{\partial K} \approx H\left(w|_\Gamma^{(\mathrm{in})}, w|_\Gamma^{(\mathrm{out})}, n_{\partial K}\right) \cdot \varphi \bigg|_{\partial K}, \tag{5.14}$$

where $w|_\Gamma^{(\mathrm{in})}$, $w|_\Gamma^{(\mathrm{out})}$ are the traces of w on ∂K from the interior and the exterior of element $K \in \mathcal{T}_h$, respectively and $H(\cdot,\cdot,\cdot)$ is a *numerical flux*, for details, see, e.g. [33] or [35]. Then with the aid of (5.8) and (5.14) we define the form

$$\bar{b}_h(w,\varphi) \equiv \sum_{\Gamma \in \mathcal{F}_h} \int_\Gamma H\left(w|_\Gamma^{(p)}, w|_\Gamma^{(n)}, n_\Gamma\right) \cdot [\varphi]_\Gamma \, \mathrm{d}S - \sum_{K \in \mathcal{T}_h} \int_K \sum_{s=1}^{d} f(w) \cdot \frac{\partial \varphi}{\partial x_s} \, \mathrm{d}x. \tag{5.15}$$

In order to employ the concept of semi-implicit schemes we need that the numerical flux H has a form suitable for a linearization. Hence, in our applications we employ the Vijayasundaram numerical flux, see [59], [33], Section 7.3 or [35], Section 3.3.4. The matrix $P(w,n)$ defined by (2.14) is diagonalizable, i.e., there exist matrices Λ and T such that

$$P(w,n) = T\Lambda T^{-1}, \ \Lambda = \mathrm{diag}\,(\lambda_1,\ldots,\lambda_{d+2}), \tag{5.16}$$

where $\lambda_1,\ldots,\lambda_{d+2}$ are the eigenvalues of P. We define the "positive" and "negative" part of P by

$$P^\pm(w,n) = T\Lambda^\pm T^{-1}, \ \Lambda^\pm = \mathrm{diag}\,(\lambda_1^\pm,\ldots,\lambda_4^\pm). \tag{5.17}$$

Then the Vijayasundaram numerical flux reads

$$H(w_1,w_2,n) \equiv P^+\left(\frac{w_1+w_2}{2},n\right)w_1 + P^-\left(\frac{w_1+w_2}{2},n\right)w_2. \tag{5.18}$$

Similarly as the Vijayasundaram numerical flux (5.18) we can apply, e.g., the Roe's type schemes [52] having also a form suitable for a linearization.

It is necessary to specify the meaning of $w|_\Gamma^{(n)}$ for $\Gamma \in \mathcal{F}_h^{DN}$. We use the approach known from the inviscid flow simulation, see, e.g., [35], [60]. For $\Gamma \in \mathcal{F}_h^{io}$ we prescribe

m_n components of w on Γ and extrapolate $m_p = d+2-m_n$ components of w from K to Γ ($\Gamma \subset \partial K$) where m_n is the number of negative eigenvalues of matrix $\mathbf{P}(w,n)$ given by (2.14). Thus, we define

$$w|_\Gamma^{(n)} = LRP(w|_\Gamma^{(p)}, w_D, \mathbf{n}_\Gamma), \tag{5.19}$$

where $LRP(\cdot,\cdot,\cdot)$ represents a solution of the *local Riemann problem* considered on edge $\Gamma \in \mathcal{F}_h^{io}$ and w_D is a given state vector (e.g. from far-field boundary conditions). For details, see [30].

For $\Gamma \in \mathcal{F}_h^w$, the impermeability condition

$$\mathbf{v} \cdot \mathbf{n} = 0 \tag{5.20}$$

is prescribed. Then in virtue of (5.14) we put

$$\int_\Gamma \mathbf{H}(w(t)|_\Gamma^{(p)}, w(t)|_\Gamma^{(n)}, \mathbf{n}_\Gamma) \cdot \boldsymbol{\varphi}\, \mathrm{d}S := \int_\Gamma \mathbf{F}_W(w(t), \mathbf{n}_\Gamma) \cdot \boldsymbol{\varphi}\, \mathrm{d}S, \quad \Gamma \in \mathcal{F}_h^W, \tag{5.21}$$

where

$$\mathbf{F}_W(w,n) \equiv (0, pn_1, \ldots, pn_d, 0)^\mathrm{T}. \tag{5.22}$$

The pressure p is expressed in the form

$$p = (\gamma-1)\left(w_{d+2} - \frac{w_2^2 + \cdots + w_{d+1}^2}{2w_1}\right), \tag{5.23}$$

following from (2.8) and (2.2) and extrapolated on Γ from K ($\Gamma \subset \partial K$) and $\mathbf{n} = (n_1, \ldots, n_d) = \mathbf{n}_\Gamma$.

The approximate solution of (CFP) is sought in the space of discontinuous piecewise polynomial functions $S_{h\mathrm{p}}$ defined by (3.5). We introduce the *semi-discrete problem*.

Definition 5.1. Function w_h is a *semi-discrete solution* of (CFP), if

a) $w_h \in C^1(0,T; S_{h\mathrm{p}})$,   (5.24)

b) $\left(\dfrac{\partial w_h(t)}{\partial t}, \boldsymbol{\varphi}_h\right) + \tilde{a}_h(w_h(t), \boldsymbol{\varphi}_h) + \bar{b}_h(w_h(t), \boldsymbol{\varphi}_h) + J_h^\sigma(w_h(t), \boldsymbol{\varphi}_h) = 0$

$$\forall \boldsymbol{\varphi}_h \in S_{h\mathrm{p}}, \ \forall t \in (0,T),$$

c) $w_h(0) = w_h^0$,

where $w_h^0 \in S_{h\mathrm{p}}$ denotes an $S_{h\mathrm{p}}$-approximation of the initial condition w^0 from (2.9).

Here $C^1(0,T; S_{h\mathrm{p}})$ is the space of continuously differentiable mappings of the interval $(0,T)$ into $S_{h\mathrm{p}}$. The problem (5.24), a) – c) exhibits a system of ordinary differential equations (ODEs) for $w_h(t)$ which has to be discretized by a suitable method.

5.3 Full time-space discretization

The ODEs system (5.24) belongs to the class of stiff problems whose solution by an explicit scheme is rather inefficient. On the other hand, a full implicit scheme leads to a necessity to solve a system of nonlinear algebraic equations at each time step which is rather expensive. Therefore, we follow the approach presented in [31] for the inviscid flow simulation where a semi-implicit time discretization was developed. Hence, we introduce a linearization of the nonlinear forms $\bar{b}_h$ and $\tilde{a}_h$ in Sections 5.3.1 and 5.3.2, respectively, and then we define the full time-space discretization of (CFP) by the so-called BDF-DGFE method.

5.3.1 Linearization of inviscid terms

By (5.15), for $w_h, \varphi_h \in S_{hp}$ we have

$$\bar{b}_h(w_h, \varphi_h) = \underbrace{-\sum_{K \in \mathcal{T}_h} \int_K \sum_{s=1}^{d} f_s(w_h) \cdot \frac{\partial \varphi_h}{\partial x_s} \mathrm{d}x}_{=:\tilde{\chi}_1(w_h, \varphi_h)} + \underbrace{\sum_{\Gamma \in \mathcal{F}_h} \int_\Gamma H\left(w|_\Gamma^{(p)}, w|_\Gamma^{(n)}, n_\Gamma\right) [\varphi]_\Gamma \mathrm{d}S}_{=:\tilde{\chi}_2(w_h, \varphi_h)}. \qquad (5.25)$$

The individual forms $\tilde{\chi}_1(\cdot, \cdot)$ and $\tilde{\chi}_2(\cdot, \cdot)$ will be linearized separately. For $\tilde{\chi}_1$, we employ the property (2.12) of the Euler fluxes and for $\bar{w}_h, w_h, \varphi_h \in S_{hp}$ define a form

$$\chi_1(\bar{w}_h, w_h, \varphi_h) \equiv \sum_{K \in \mathcal{T}_h} \int_K \sum_{s=1}^{d} A_s(\bar{w}_h(x)) w_h(x) \cdot \frac{\partial \varphi_h(x)}{\partial x_s} \mathrm{d}x. \qquad (5.26)$$

The linearization of the term $\tilde{\chi}_2$ can be carried out in a simple way, when H in (5.25) is chosen, for example, as the Vijayasundaram numerical flux (5.18). Let $\bar{w}_h, w_h, \varphi_h \in S_{hp}$, we put

$$\tilde{\chi}_2(\bar{w}_h, w_h, \varphi_h) \equiv \sum_{\Gamma \in \mathcal{F}_h} \int_\Gamma \left[P^+(\langle \bar{w}_h \rangle, n) w_h|_\Gamma^{(p)} + P^-(\langle \bar{w}_h \rangle, n) w_h|_\Gamma^{(n)} \right] \cdot [\varphi_h] \mathrm{d}S, \qquad (5.27)$$

where $\langle \bar{w}_h \rangle$ is given by (3.6).

It is necessary to pay a special attention to $w_h|_\Gamma$ for $\Gamma \in \mathcal{F}_h^{DN}$. For $\Gamma \in \mathcal{F}_h^w$ we employ approximation (5.21). The vector F_W defined by (5.22) is a nonlinear function of w and its linearization is given with the aid of the Taylor expansion by

$$\begin{aligned} F_W(w_h, n) \approx \tilde{F}_W(\bar{w}_h, w_h, n) &\equiv F_W(\bar{w}_h, n) + DF_W(\bar{w}_h, n)(w_h - \bar{w}_h) \\ &= DF_W(\bar{w}_h, n) w_h, \end{aligned} \qquad (5.28)$$

where

$$DF_W(w, n) \equiv (\gamma - 1) \begin{pmatrix} 0 & 0 & \dots & 0 & 0 \\ (v_1^2 + \dots + v_d^2)n_1/2 & -v_1 n_1 & \dots & -v_d n_1 & n_1 \\ \vdots & \vdots & \ddots & \vdots & \vdots \\ (v_1^2 + \dots + v_d^2)n_d/2 & -v_1 n_d & \dots & -v_d n_d & n_d \\ 0 & 0 & \dots & 0 & 0 \end{pmatrix} \qquad (5.29)$$

is obtained by the differentiation of function F_W given by (5.22) with respect to $w = (w_1,\ldots,w_d)$. Here $n = (n_1,\ldots,n_d)$, $v_j = w_{j+1}/w_1$, $j = 1,\ldots,d$. The last equality in (5.28) follows from (2.12) which implies $F_W(\bar{w}_h,n) = DF_W(\bar{w}_h,n)\bar{w}_h$.

Then we put

$$
\chi_2(\bar{w}_h,w_h,\boldsymbol{\varphi}_h) \tag{5.30}
$$
$$
\equiv \sum_{\Gamma\in\mathcal{F}_h^I}\int_\Gamma\left(P^+\left(\langle\bar{w}_h\rangle,n\right)w_h|_\Gamma^{(p)}+P^-\left(\langle\bar{w}_h\rangle,n\right)w_h|_\Gamma^{(n)}\right)\cdot[\boldsymbol{\varphi}_h]\mathrm{d}S
$$
$$
+ \sum_{\Gamma\in\mathcal{F}_h^{io}}\int_\Gamma\left(P^+\left(\langle\bar{w}_h\rangle,n\right)w_h|_\Gamma^{(p)}+P^-\left(\langle\bar{w}_h\rangle,n\right)\bar{w}_h|_\Gamma^{(n)}\right)\cdot[\boldsymbol{\varphi}_h]\mathrm{d}S
$$
$$
+ \sum_{\Gamma\in\mathcal{F}_h^w}\int_\Gamma\tilde{F}_W(\bar{w}_h,w_h,n_{ij})\cdot\boldsymbol{\varphi}\,\mathrm{d}S,
$$

where, in virtue (5.19),

$$
\bar{w}|_\Gamma^{(n)} = LRP(\bar{w}|_\Gamma^{(p)},w_D,n_\Gamma),\quad \Gamma\in\mathcal{F}_h^{io}. \tag{5.31}
$$

Finally, we define the form

$$
b_h(\bar{w}_h,w_h,\boldsymbol{\varphi}_h) \equiv -\chi_1(\bar{w}_h,w_h,\boldsymbol{\varphi}_h) + \chi_2(\bar{w}_h,w_h,\boldsymbol{\varphi}_h), \tag{5.32}
$$

where χ_1 and χ_2 are given by (5.26) and (5.30), respectively. The form b_h is linear with respect to the second and third variable and consistent with $\bar{b}_h$ by

$$
\bar{b}_h(w_h,\boldsymbol{\varphi}_h) = b_h(w_h,w_h,\boldsymbol{\varphi}_h)\quad \forall w_h,\boldsymbol{\varphi}_h\in S_{h\mathrm{p}}. \tag{5.33}
$$

5.3.2 Linearization of viscous terms

In virtue of (5.7), for $\bar{w}_h,w_h,\boldsymbol{\varphi}_h\in S_{h\mathrm{p}}$ we define the form

$$
\begin{aligned}
a_h(\bar{w}_h,w_h,\boldsymbol{\varphi}_h) &= \sum_{K\in\mathcal{T}_h}\int_K\sum_{s=1}^d\left(\sum_{k=1}^d K_{s,k}(\bar{w}_h)\frac{\partial w_h}{\partial x_k}\right)\cdot\frac{\partial\boldsymbol{\varphi}_h}{\partial x_s}\mathrm{d}x \\
&\quad - \sum_{\Gamma\in\mathcal{F}_h^{ID}}\int_\Gamma\sum_{s=1}^d\left\langle\sum_{k=1}^d K_{s,k}(\bar{w}_h)\frac{\partial w_h}{\partial x_k}\right\rangle n_s\cdot[\boldsymbol{\varphi}_h]\mathrm{d}S \\
&\quad - \eta\sum_{\Gamma\in\mathcal{F}_h^{ID}}\int_\Gamma\sum_{s=1}^d\left\langle Q_s(\bar{w}_h,\nabla\bar{w}_h,\boldsymbol{\varphi}_h,\nabla\boldsymbol{\varphi}_h)\right\rangle n_s\cdot[w_h]\mathrm{d}S \\
&\quad + \eta\sum_{\Gamma\in\mathcal{F}_h^D}\int_\Gamma\sum_{s=1}^d Q_s(\bar{w}_h,\nabla\bar{w}_h,\boldsymbol{\varphi}_h,\nabla\boldsymbol{\varphi}_h)n_s\cdot w_B\mathrm{d}S,
\end{aligned} \tag{5.34}
$$

which is linear with respect to its second and third components. Moreover, it is consistent with $\tilde{a}_h(\cdot,\cdot)$ by

$$
\tilde{a}_h(w_h,\boldsymbol{\varphi}_h) = a_h(w_h,w_h,\boldsymbol{\varphi}_h)\quad \forall w_h,\boldsymbol{\varphi}_h\in S_{h\mathrm{p}}. \tag{5.35}
$$

5.3.3 BDF-DGFE semi-implicit scheme

The main idea of the semi-implicit discretization is to treat the linear parts of forms a_h and b_h (represented by their second and their arguments) implicitly and their nonlinear parts (represented by their first arguments) explicitly. In order to obtain a sufficiently stable and accurate approximation with respect to the time coordinate, we use the *backward difference formula* (BDF), see, e.g., [36], for the solution the ODE problem (5.24), a) – c). Moreover, for the nonlinear parts of $a_h(\cdot,\cdot,\cdot)$ and $b_h(\cdot,\cdot,\cdot)$, we employ a suitable explicit higher order extrapolation which preserves a given order of accuracy and does not destroy the linearity of the problem at each time level. This approach is often called *extrapolated BDF* method and it was introduced and investigated in [16] and [58] for the second order scheme. In [29], we analysed the extrapolated BDF-DGFE method applied to the space discretization (4.16), a)–c) of the model problem (4.1).

Let $0 = t_0 < t_1 < \cdots < t_r = T$ be a partition of the interval $(0,T)$ and $\tau_k \equiv t_{k+1} - t_k$, $k = 0,1,\ldots,r-1$. In order to simplify the notation, we put

$$c_h(\bar{w}_h, w_h, \varphi_h) \equiv a_h(\bar{w}_h, w_h, \varphi_h) + b_h(\bar{w}_h, w_h, \varphi_h) + J_h^\sigma(w_h, \varphi_h), \quad \bar{w}_h, w_h, \varphi_h \in S_{hp}. \quad (5.36)$$

Definition 5.2. We define the *approximate solution* of (CFP) the set of functions w_h^k, $k = 1,\ldots,r$, satisfying the conditions

a) $\quad w_h^{k+1} \in S_{hp}$, $\hspace{7cm}$ (5.37)

b) $\quad \dfrac{1}{\tau_k}\left(\displaystyle\sum_{l=0}^{n}\alpha_l w_h^{k+1-l}, \varphi_h\right) + c_h\left(\displaystyle\sum_{l=1}^{n}\beta_l w_h^{k+1-l}, w_h^{k+1}, \varphi_h\right) = 0$

$$\forall \varphi_h \in S_{hp},\ k = n-1,\ldots,r-1,$$

c) $\quad w_h^0$ is S_{hp} approximation of w^0,

d) $\quad w_h^l \in S_{hp}$, $l = 1,\ldots,n-1$ are given by a suitable one-step method,

where $n \geq 1$ is the degree of the BDF scheme, the coefficients α_l, $l = 0,\ldots,n$ and β_l, $l = 1,\ldots,n$ depend on time steps τ_{k-l}, $l = 0,\ldots,n$. We call this approach the *BDF-DGFE method*.

The relations for the coefficients α_l, $l = 0,\ldots,n$ and β_l, $l = 1,\ldots,n$ can be found in [36, Section III.5] or [28] for $n = 1,2,3$ and their values for constant time step $\tau_k = \tau$, $k = 1,\ldots,r$ are given in Table 1.

n	$\alpha_l,\ l=0,\ldots,n$				$\beta_l,\ l=1,\ldots,n$		
1	1,	-1			1		
2	$\frac{3}{2}$,	-2,	$\frac{1}{2}$		2,	-1	
3	$\frac{11}{6}$,	-3,	$\frac{3}{2}$,	$-\frac{1}{3}$	3,	-3,	1

Table 1: Values of coefficients α_l and β_l for constant time step

The problem (5.37), a) – d) represents a system of linear algebraic equations for each $k = n-1,\ldots,r-1$ which is solved by a suitable linear algebra solver.

Remark 5.1. There is a natural question how accurate and stable is the proposed BDF-DGFE method (5.37). This method was analysed for the case of a scalar convection-diffusion equation with a nonlinear convective term and a linear diffusive term in [29]. Assuming that the exact solution is sufficiently regular, we derived a priori error estimates (for the SIPG version)

$$
\begin{aligned}
\|u-u_h\|_{L^\infty(0,T;L^2(\Omega))} &\leq\ C\left(h^{p+1}+\tau^n\right), \\
|u-u_h|_{L^2(0,T;H^1(\Omega,\mathcal{T}_h))} &\leq\ C\left(h^p+\tau^n\right),
\end{aligned}
\tag{5.38}
$$

where u is the exact solution, u_h the approximate solution obtained by the n-step BDF-DGFE method ($n=1,2,3$), $p\geq 1$ is the degree of polynomial approximation, h is the mesh size, τ is the size of time step and C is a constant independent of h and τ. The estimates (5.38) were obtained without any restriction on the size of the time step, for more details see [29].

On the other hand, numerical analysis of the BDF-DGFE method (5.37) applied to the system of the Navier-Stokes equations is rather complicated. However, numerical experiments presented in this paper indicate that this scheme is sufficiently stable and accurate, see Section 6.1 (Figure 5), where the stability of the BDF-DGFE method is demonstrated and Sections 6.2 and 6.3 where comparisons of an accuracy of the BDF-DGFE method with respect to the space and time are presented.

Remark 5.2. It is possible to consider a generalization of the BDF-DGFE method (5.37), a) - d), which is based on the replacing the condition (5.37), b) by

$$
\text{b1)}\quad w_h^{k+1,0}\equiv\sum_{l=1}^n\beta_l w_h^{k+1-l}\quad\text{or}\quad w_h^{k+1,0}\equiv w_h^k,
\tag{5.39}
$$

$$
\text{b2)}\quad w_h^{k+1,m}\in S_{h\mathsf{p}},\quad m=1,\dots,\bar{m}_{k+1},
$$

$$
\text{b3)}\quad \left(\alpha_0 w_h^{k+1,m},\varphi_h\right)+\tau_k c_h\left(w_h^{k+1,m-1},w_h^{k+1,m},\varphi_h\right)=-\left(\sum_{l=1}^n\alpha_l w_h^{k+1-l},\varphi_h\right)
$$

$$
\forall\varphi_h\in S_{h\mathsf{p}},\ m=1,\dots,\bar{m}_{k+1},\ k=n-1,\dots,r-1,
$$

$$
\text{b4)}\quad w_h^{k+1}\equiv w_h^{k+1,\bar{m}_{k+1}},
$$

where $\bar{m}_{k+1}\geq 2$ denotes the number of inner loops. The value $\bar{m}_{k+1}$ is chosen usually in such a way that

$$
\|w_h^{k+1,\bar{m}_{k+1}}-w_h^{k+1,\bar{m}_{k+1}-1}\|\leq\omega,
\tag{5.40}
$$

where $\omega>0$ is a given tolerance and $\|\cdot\|$ is a suitable norm. The resulting "fully-implicit" numerical scheme (5.39), b1)– b4), (5.37), a), c), d) belongs to the Newton-like methods, which are based on a suitable approximation of the Jacobi matrix.

The fully-implicit scheme should be more accurate and stable than the semi-implicit one. On the other hand, fully-implicit scheme is more expensive since it requires solution

of $\bar{m}_{k+1}$ linear algebraic problems at the time level $k+1$. However, for increasing m ($1 \le m \le \bar{m}_{k+1}$) the solution of the corresponding linear algebraic problem is faster and faster since we have better and better initial approximation of the solution.

Nevertheless, we carried out several numerical experiments (not presented in this paper) which indicate that fully-implicit scheme does not exhibits any gain in the accuracy and the stability in comparison with the semi-implicit one.

Remark 5.3. Another similar approach of the solving of the semi-discrete problem (5.24) is the solution of the linearised problem by an implicit Runge-Kutta method. Although the implicit Runge-Kutta methods are sufficiently stable they are not so efficient as the BDF schemes. It follows from the fact that the m-stage ($m \ge 1$) implicit Runge-Kutta scheme needs to solve m linear algebraic problems at each time step whereas the m-step BDF requires the solution only of one linear algebraic problem for any $m \ge 1$.

5.4 Implementation aspects of BDF-DGFE method

Linear algebraic system solver As we mentioned in the previous section, problems (5.37), a)–d) represents a system of linear algebraic equations. Let $\{\boldsymbol{\psi}_l\}_{l=1}^{\mathrm{dof}}$ represent a basis of the space of vector-valued discontinuous piecewise polynomial functions $S_{h\mathrm{p}}$ defined by (3.5), where dof denotes the dimension of $S_{h\mathrm{p}}$. Then a function $\boldsymbol{w}_h^k \in S_{h\mathrm{p}}$ can be written in the form

$$\boldsymbol{w}_h^k(x) = \sum_{l=1}^{\mathrm{dof}} \xi_k^l \boldsymbol{\psi}_l(x), \quad x \in \Omega, \, k=0,1,\dots,r, \tag{5.41}$$

where $\xi_k^l \in I\!\!R$, $l=1,\dots,\mathrm{dof}$, $k=0,\dots,r$. Moreover, for $\boldsymbol{w}_h^k \in S_{h\mathrm{p}}$ we define the vector of its basis coefficients by

$$\boldsymbol{W}^k \equiv \left(\xi^{k,1}, \, \xi^{k,2}, \dots, \xi^{k,\mathrm{dof}} \right) \in I\!\!R^{\mathrm{dof}}, \quad k=0,1,\dots,r. \tag{5.42}$$

Then the linear algebraic problem (5.37) can be written in the matrix form

$$\left(\alpha_0 \boldsymbol{M} + \tau_k \boldsymbol{C}^k \right) \boldsymbol{W}^k = \boldsymbol{q}^k, \quad k=n,\dots,r, \tag{5.43}$$

where matrix $\boldsymbol{M}$ is the *mass matrix* given by

$$\boldsymbol{M} = \{\boldsymbol{M}^{(i,j)}\}_{i,j=1}^{\mathrm{dof}}, \qquad \boldsymbol{M}^{(i,j)} \equiv \int_\Omega \boldsymbol{\psi}_i \cdot \boldsymbol{\psi}_j \mathrm{d}x, \quad i,j=1,\dots,\mathrm{dof}, \tag{5.44}$$

$\boldsymbol{C}_k$ is a the matrix corresponding to form $c_h(\cdot,\cdot,\cdot)$ defined by

$$\boldsymbol{C}^k = \boldsymbol{C}^k(\boldsymbol{W}^{k-1}, \boldsymbol{W}^{k-2},\dots,\boldsymbol{W}^{k-n}), \tag{5.45}$$

$$\boldsymbol{C}^k \equiv \{\boldsymbol{C}_k^{(i,j)}\}_{i,j=1}^{\mathrm{dof}}, \quad \boldsymbol{C}_k^{(i,j)} \equiv c_h \left(\sum_{l=1}^n \beta_l \boldsymbol{w}_h^{k-l}, \, \boldsymbol{\psi}_i, \, \boldsymbol{\psi}_j \right), \, i,j=1,\dots,\mathrm{dof},$$

and $q^k \in I\!R^{\mathrm{dof}}$ represents the right-hand-side of (5.37)given by

$$q^k = q^k(W^{k-1}, W^{k-2}, \ldots, W^{k-n}) = \{q^{k,i}\}_{i=1}^{\mathrm{dof}}, \quad q^{k,i} \equiv -\left(\sum_{l=1}^{n} \alpha_l w_h^{k-l}, \, \psi_i\right), \quad (5.46)$$

The linear algebraic problem (5.43) should be numerically solved at each time level t_k, $k=n, \ldots, r$. It is possible to use a direct solver which is more efficient for not too large dof (usually dof$\approx 10^4 - 10^5$). For larger systems, it is suitable to use some iterative solvers. We employ the restarted GMRES solver with the block diagonal preconditioning. The restart was carried out after 45 iterations. The iterative process was stopped if the discrete ℓ^2-norm of the residuum was smaller than 10^{-5}. Numerical simulations of steady as well as unsteady flow problems indicate that this choice is sufficient, i.e., smaller value of the tolerance does not cause any increase of accuracy and stability of the method.

Choice of shape functions We dealt with this aspect in [21]. We construct orthogonal basis of $S_{h\mathrm{p}}$ by the Grant-Schmidt orthogonalization process on each element $K \in \mathcal{T}_h$ separately. Although it is a known fact, that this algorithm is ill-conditioned, we do not observed any problem with the stability of the Grant-Schmidt orthogonalization. It is caused by the fact that the dimension of the finite element space on each element is small and moreover if the basis is not (exactly) orthogonal it does not mind.

The orthogonality of the basis of $S_{h\mathrm{p}}$ implies that the mass matrix M given by (5.44) is (up to round off errors) diagonal and then for small time step τ_k the linear algebraic problem (5.43) can be solved very fast in few iterations. However, for increasing size of the time step this advantage is diminishing, see Section 6.1, the comment to Figure 5 (left).

Choice of the time step The time steps τ_k, $k = 0, 1, \ldots$ are chosen adaptively. We use the identical technique as in [28] where the inviscid flow simulation was treated. This approach is based on a use of two semi-implicit multistep formulae of the same order of accuracy and from their difference we estimate the local discretization error and propose a new time step. However, this adaptive method optimises the number of time steps but no the computational time.

The optimal choice of the time step with respect to the computational time (including setting of suitable stopping condition for the linear algebra solver) is quite open and it will be a subject of further research.

Representation of non-polygonal boundaries In order to obtain a physically admissible distribution of physical quantities on non-polygonal boundaries, we employ the super-parametric finite elements, see [23].

Choice of the penalty parameter σ The penalty coefficient σ appearing in the definition of $J_h^\sigma(\cdot,\cdot)$ is given by relation (5.10) which is a natural generalization of (4.7). In the case of the *model scalar equation*, the value $C_W > 0$ in (4.7) can be set by from the theory. Whereas, for the NIPG variant of the DGFE method, it is sufficient to put $C_W = 1$, for the SIPG and the IIPG variants, the value of C_W should be sufficiently large, the limit values were derived analytically, see, e.g., [22], [24], [27], [41].

However, for the *Navier-Stokes equations* the situation is more complicated since a relevant mathematical theory is missing. Therefore, the appropriate values of C_W have to be found experimentally. This aspect together with the influence of the size of C_W to the solution is studied in Section 6.

6   Numerical examples

In this section we present three two-dimensional numerical examples. The first one is a basic benchmark of steady viscous flow around a flat plate. The second and third ones represent a steady and an unsteady flows around NACA 0012 profile, respectively.

6.1   Blasius problem

We consider the laminar flow on the adiabatic flat plate $\{(x_1,x_2);\ 0 \le x_1 \le 1, x_2 = 0\}$ characterised by the freestream Mach number $M = 0.1$ and the Reynolds number $Re = 10^4$. The computation domain is viewed in Figure 3, where two used triangular grids are plotted together with their details around the leading edge. We prescribe the adiabatic boundary conditions (2.10), c) at the flat plate, the outflow boundary conditions (2.10), b) at $\{(x_1,x_2);\ x_1 = 1, -1.5 \le x_2 \le 1.5\}$ and the inflow boundary conditions (2.10), a) on the rest of the boundary.

We seek the steady state solution by the time stabilization approach where the computational process is carried out for "$t \to \infty$". As a stopping criterion we employ the condition

$$\text{res}(k) \equiv \frac{\|r^k\|_{L^2(\Omega)}}{\|r^1\|_{L^2(\Omega)}} \le \bar\omega, \tag{6.1}$$

where $\bar\omega > 0$ is a prescribed tolerance and $r^k \in S_{h\mathsf{p}}$ is an approximation of $\frac{\partial}{\partial t} w(t_k)$, $t_k \in (0,T)$ given by

$$r^k \equiv \frac{1}{\tau_{k-1}} \left(w_h^k - w_h^{k-1} \right). \tag{6.2}$$

In the computations presented within Section 6.1 we put $\bar\omega = 10^{-6}$.

6.1.1   Stability of the method

We compared the NIPG, IIPG, SIPG variants of the DGFEM using piecewise linear, quadratic and cubic space approximation. Our aim is to find a suitable value of the constant C_W in
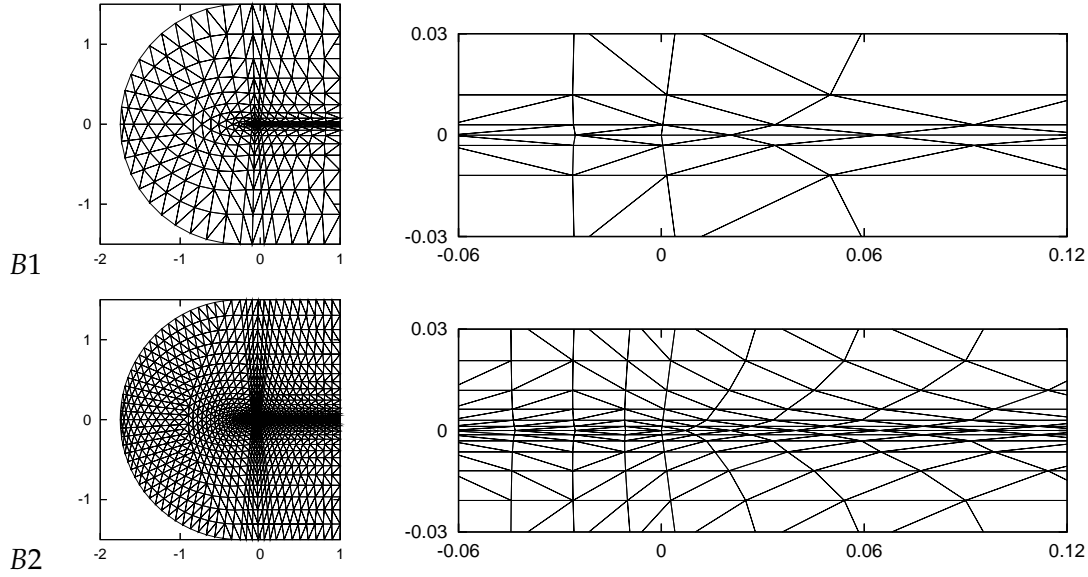
Figure 3: Blasius problem, computational grids $B1$ and $B2$, the coarser one $B1$ having 662 elements (top) and the finer one $B2$ having 2648 elements (bottom), the whole computational domain (left) and their details around the leading edge (right)

(5.10) which ensures the stability of the scheme, i.e., a convergence to the steady-state solution. Firstly, we carried out computations for the values of $C_W = 1, 5, 25, 125, 625, 3125$ and consequently, several additional values of C_W were chosen in order to find a limit value of C_W. These results obtained on the grid $B1$ are shown in Table 2, where an indication of a convergence of the appropriate variant of the DGFEM with a given value C_W is marked, namely,

- "convergence" (C), i.e., the stopping condition (6.1) was achieved after less than 200 time steps,

- "quasi-convergence" (qC), i.e., the stopping condition (6.1) was achieved after more than 200 time steps,

- "no-convergence" (NC), i.e., the stopping condition (6.1) was not achieved after 500 time steps.

The "quasi-convergence" in fact means that the appropriate value C_W is just under the limit value ensuring a reasonable convergence to the steady-state solution.

From Table 2 we found that

- NIPG variant converges for any $C_W \geq 1$ independently on the degree of polynomial approximation,

C_W	NIPG			IIPG			SIPG		
	P_1	P_2	P_3	P_1	P_2	P_3	P_1	P_2	P_3
1	C	C	C	C	NC	NC	N	N	N
5	C	C	C	C	C	NC	N	N	N
10	-	-	-	-	C	C	-	-	-
25	C	C	C	C	C	C	N	N	N
100	-	-	-	-	-	-	N	-	-
125	C	C	C	C	C	C	C	N	N
150	-	-	-	-	-	-	C	-	-
250	-	-	-	-	-	-	-	N	-
300	-	-	-	-	-	-	-	qC	-
400	-	-	-	-	-	-	-	C	N
500	-	-	-	-	-	-	-	C	N
625	C	C	C	C	C	C	C	C	qC
1 000	-	-	-	-	-	-	-	-	C
3 125	C	C	C	C	C	C	C	C	C

Table 2: Blasius problem, the convergence (C), non-convergence (NC) or quasi-convergence (qC) of the NIPG, IIPG and SIPG variants of the DGFEM for P_1, P_2 and P_3 approximations for different values of C_W (symbol "-" means that the appropriate combination of the method, the degree of approximation and the value of C_W was not tested)

- IIPG variant requires higher values of C_W for P_2 and P_3 approximations, namely $C_W=5$ and $C_W=10$ are sufficient, respectively. On the other hand, P_1 approximation converges for any $C_W \geq 1$.

- SIPG variant requires significantly higher values of C_W. We observe that $C_W \geq 125$ for P_1, $C_W \geq 400$ for P_1 and $C_W \geq 1000$ for P_3. This is in a good agreement with the theoretical results from [41] carried out for a scalar quasilinear elliptic problem, where the dependence $C_W = cp^2$, $c>0$ is employed (p denotes the polynomial degree of approximation).

Figure 4 shows the histories of convergence to the steady-state solution (i.e., the dependence of $\mathrm{res}(k)$ on k) for some interesting cases from Table 2.

Furthermore, it is interesting to observe the size of time steps adaptively chosen by the BDF-DGFE method in a possible comparison with a fictitious explicit time discretization method. Hence, we define the so-called cfl-value by

$$\mathrm{cfl}(k) \equiv \tau_k \Lambda(w_h^k), \quad k=1,\ldots,r, \tag{6.3}$$

where $\Lambda(\cdot)$ is an approximation of the maximal eigenvalue of the ODE system (5.24) given by

$$\Lambda(w_h^k) \equiv \max \left(\min_{\substack{K \in \mathcal{T}_h \\ \Gamma \subset \partial K}} \frac{|K|}{r_\Gamma(w_h^k, n)|\Gamma|}, \ \min_{K \in \mathcal{T}_h} \frac{|K|}{Re} \right) \tag{6.4}$$
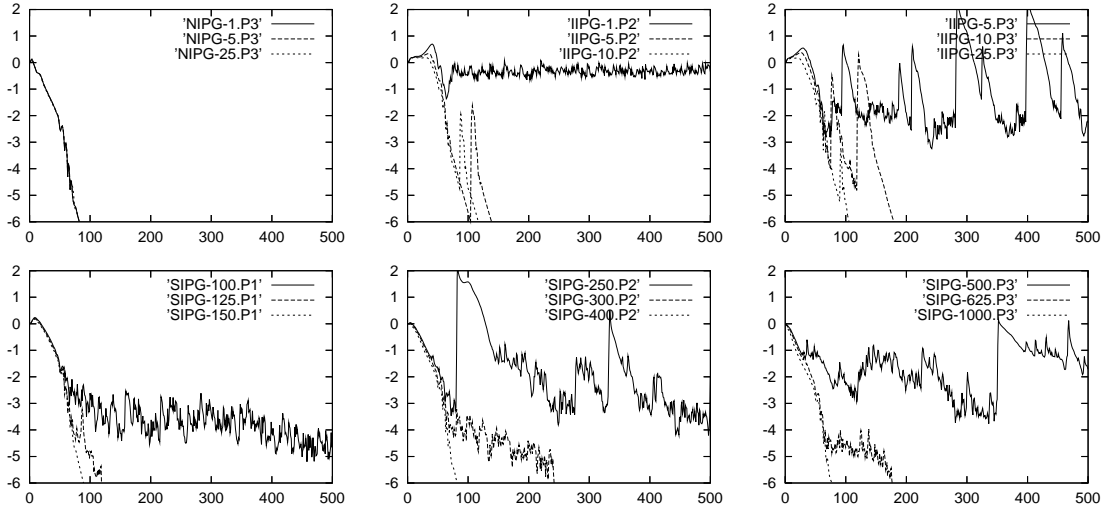
Figure 4: Blasius problem, the histories of convergence for some computations from Table 2, (e.g., 'NIPG-625.P3' means the NIPG variant of DGFEM with $C_W = 625$ and P_3 approximation)

where $r_\Gamma(\boldsymbol{w}_h^k, \boldsymbol{n})$ denotes the spectral radius of the matrix $\boldsymbol{P}(\boldsymbol{w}_h^k, \boldsymbol{n})|_\Gamma$ given by (2.14) and Re is the Reynolds number. Numerical experiments show that an explicit time scheme is stable if $\mathrm{cfl}(k) \leq 1$, see, e.g., [20, relation (70)] or [33].

Figure 5 (left) shows a typical dependence of the $\mathrm{cfl}(k)$ quantity on t_k, $k = 0,\ldots,r$. We observe that the cfl-value exponentially increases for $k = 1,2\ldots,$. This indicates that the semi-implicit BDF-DGFEM (5.37), a) - d) is practically unconditionally stable. Figure 5 (right) shows the corresponding numbers of GMRES iterations necessary to solve the linear algebra problem (5.43) at each time step. We observed that the increasing size of the time step τ_k requires higher number of iterations. However, if the numerical solution is close to the steady state one then the number of GMRES iterations starts decreasing. It is caused by the fact that the initial guess of the solution of problem (5.43) is very close to the resulting solution.

Remark 6.1. The number of GMRES iterations is rather very high and hence the presented numerical scheme is not very efficient. It would be suitable to use a more efficient linear algebra solver. A promising seems to be an application of the BiCGSTAB method with an updating technique for the ILU($\star$) preconditioners. This approach was developed in [11], where an implicit finite volume discretization of an inviscid compressible flow was considered. Our preliminary numerical experiments give significantly smaller number of iterations.
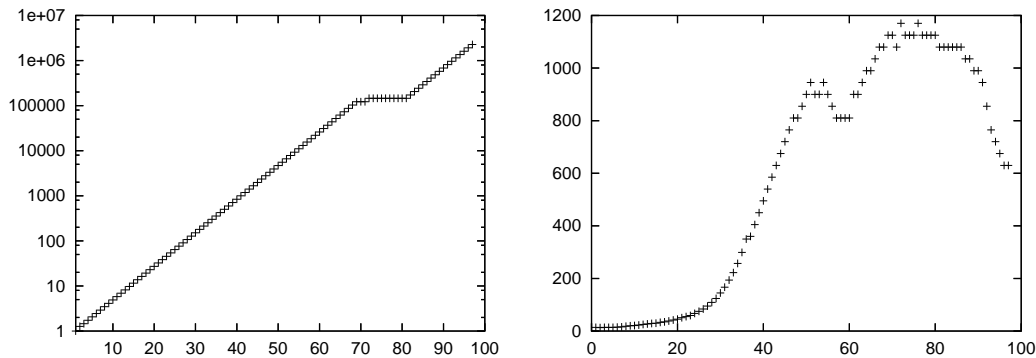
Figure 5: Blasius problem, a typical dependence of the cfl(k)-value (left) and the number of GMRES iterations (right) on the number of time steps

6.1.2 Accuracy of the method

We compared the numerical solutions with the "theoretical" one, which can be obtained from the well-known Blasius problem represented by an incompressible flow along a flat plate. Therefore, we introduce the non-dimensional velocities in the stream-direction and in the normal to stream direction by

$$v_1^\star \equiv \frac{v_1(\eta)}{|v_\infty|} \qquad \text{and} \qquad v_2^\star \equiv \sqrt{Re_x}\frac{v_2(\eta)}{|v_\infty|}, \tag{6.5}$$

respectively, where

$$\eta \equiv \sqrt{Re_x}\frac{x_2}{x_1}, \qquad Re_x \equiv |v_\infty|Re\,x_1, \tag{6.6}$$

Re is the Reynolds number and v_∞ is the free-stream velocity.

Figures 6 – 9 shows the velocity profiles $v_1^\star$ and $v_2^\star$ obtained by P_1, P_2 and P_3 approximations on meshes $B1$ and $B2$ at $x_1=0.1$, $x_1=0.3$ and $x_1=0.5$ in comparison with the exact solution. We employed the NIPG technique with $C_W=25$. The velocity profiles obtained by the SIPG and IIPG variants are almost identical. We observed very accurate capturing of the $v_1^\star$-profile and a reasonable capturing of the $v_2^\star$-profile. An increase of the accuracy for an increasing degree of approximation and a decreasing mesh size is evident.

Moreover, Figure 10 shows the comparison of the computed skin friction coefficient c_f achieved by P_1, P_2 and P_3 approximations on meshes $B1$ and $B2$ with the exact solution given by the Blasius formula. We observed a good agreement with the Blasius solution. However, P_2 and P_3 approximations give in fact the same value of c_f at the first element on the flat plate. Similar results were obtained in [6, Fig. 2] where the difference among P_1, P_2 and P_3 approximations on the first cell of the flat plate is almost negligible. We suppose that it can be caused by the singularity of the solution at $x_1 = x_2 = 0$ which decreases the local order of accuracy of the DGFE method. This phenomenon was numerically verified for a scalar nonlinear convection-diffusion equation in [26].
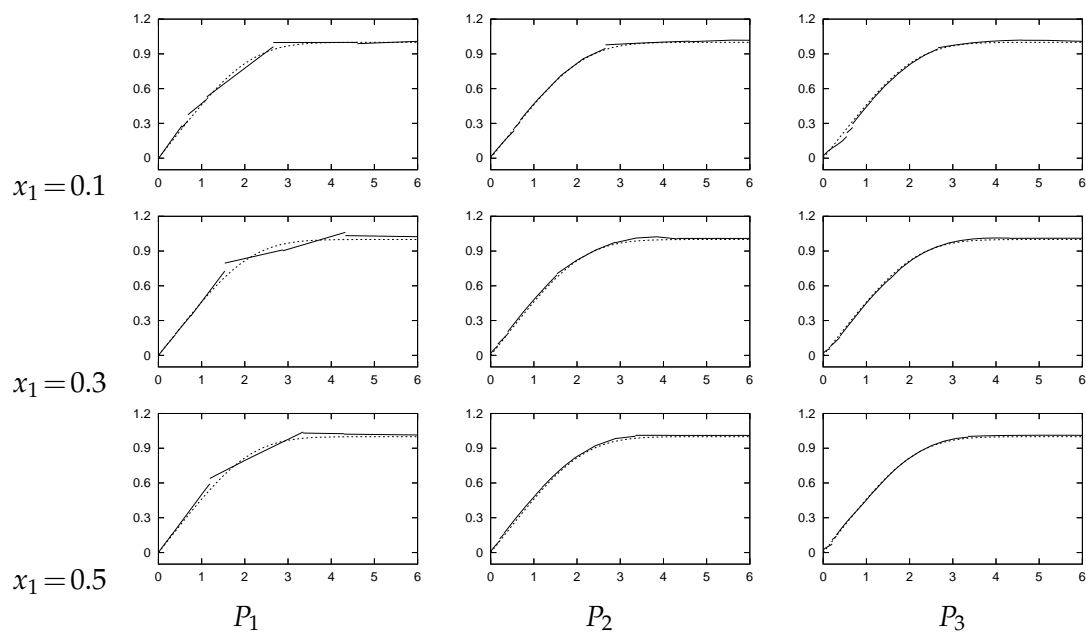
Figure 6: Blasius problem, mesh $B1$, velocity profiles $v_1^\star = v_1^\star(\eta)$ for P_1, P_2 and P_3 approximations at $x_1 = 0.1$, $x_1 = 0.3$ and $x_1 = 0.5$ in comparison with the exact solution (dotted lines)
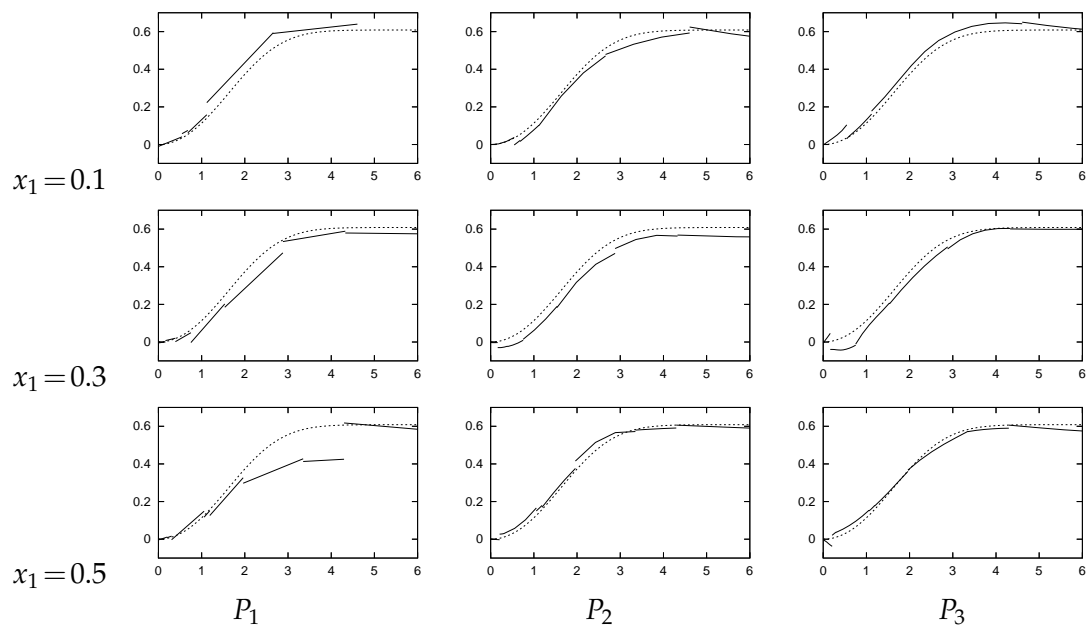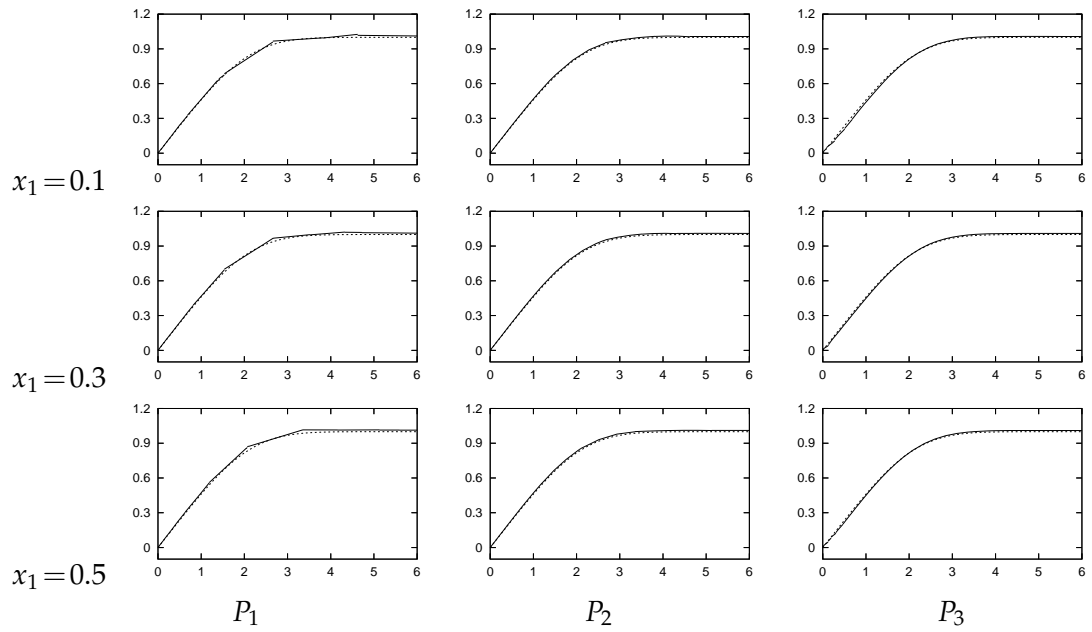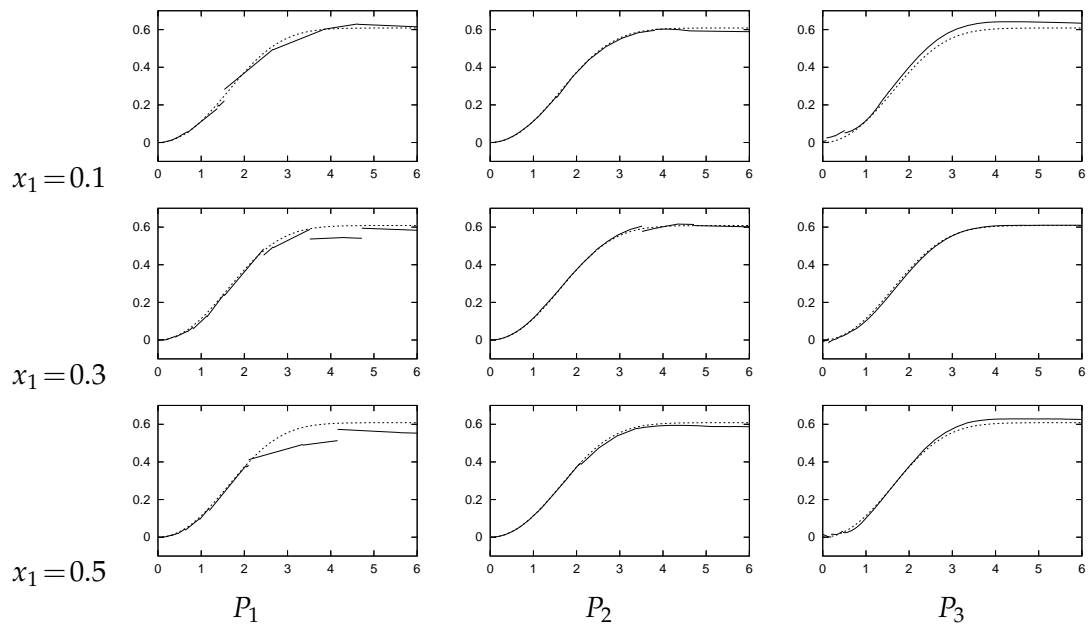

Figure 7: Blasius problem, mesh $B1$, velocity profiles $v_2^\star = v_2^\star(\eta)$ for P_1, P_2 and P_3 approximations at $x_1 = 0.1$, $x_1 = 0.3$ and $x_1 = 0.5$ in comparison with the exact solution (dotted lines)

Figure 8: Blasius problem, mesh $B2$, velocity profiles $v_1^\star = v_1^\star(\eta)$ for P_1, P_2 and P_3 approximations at $x_1 = 0.1$, $x_1 = 0.3$ and $x_1 = 0.5$ in comparison with the exact solution (dotted lines)

Figure 9: Blasius problem, mesh $B2$, velocity profiles $v_2^\star = v_2^\star(\eta)$ for P_1, P_2 and P_3 approximations at $x_1 = 0.1$, $x_1 = 0.3$ and $x_1 = 0.5$ in comparison with the exact solution (dotted lines)
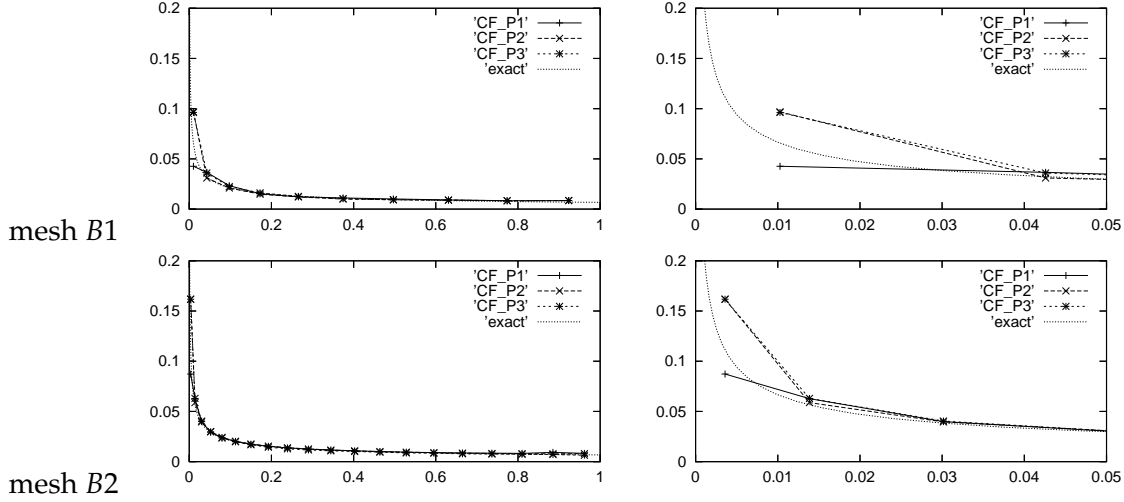
Figure 10: Blasius problem, skin friction coefficient computed on meshes $B1$ and $B2$ by P_1 ('P_1'), P_2 ('P_2') and P_3 ('P_3') approximation in comparison with the Blasius formula ('exact'), distributions along the whole plate (left), their details around the leading edge (right)

6.2 Steady-state flow around NACA0012 profile

In Section 6.1, we studied the influence of the value of the penalty parameter C_W introduced in (5.10) to the stability of the NIPG, IIPG and SIPG variants of the BDF-DGFE method (5.37). We do not observed any essential influence of C_W to, e.g., the velocity profiles. Nevertheless, the influence of C_W to the numerical solution should be investigated by a quantitative characteristic of the flow. Hence, we consider a flow around the profile NACA0012 at the free stream Mach number $M=0.5$, the angle of attack $\alpha=0°$ and Reynolds number $Re=5000$. The walls of the profile are adiabatic. The Reynolds number is near to the upper limit for the steady laminar flow. A characteristic feature of this flow problem is the separation of the flow occurring near to the trailing edge.

We carried out computations on a set of six successively generated grids $N1 - N6$ from [1]. Figure 11 shows these grids around the NACA profile and their zooms around the trailing and leading edges. The numbers of elements ($=\#\mathcal{T}_h$) and mesh sizes ($=1/\sqrt{\#\mathcal{T}_h}$) of grids $N1 - N6$ are shown in Table 3 (top). We investigated a "convergence" of the drag coefficient c_D for "$h \to 0$" for the NIPG variant with several choices of C_W. (We observed the same behaviour as well as for the IIPG and SIPG techniques.) The values of c_D are presented in Table 3 and also visualised in Figure 12. We easily observe a non-negligible dependence of c_D on C_W on coarser grids but for increasing number of elements $\#\mathcal{T}_h$ the influence of C_W to c_D decreases and c_D converges to an asymptotic value. All values of c_D obtained on the finest employed meshes differ of 0.00113 ($\approx 2\%$ of the value c_D) for P_1 approximation, 0.00027 ($\approx 0.5\%$) for P_2 approximation and 0.00024 ($\approx 0.5\%$) for P_3 approximation.
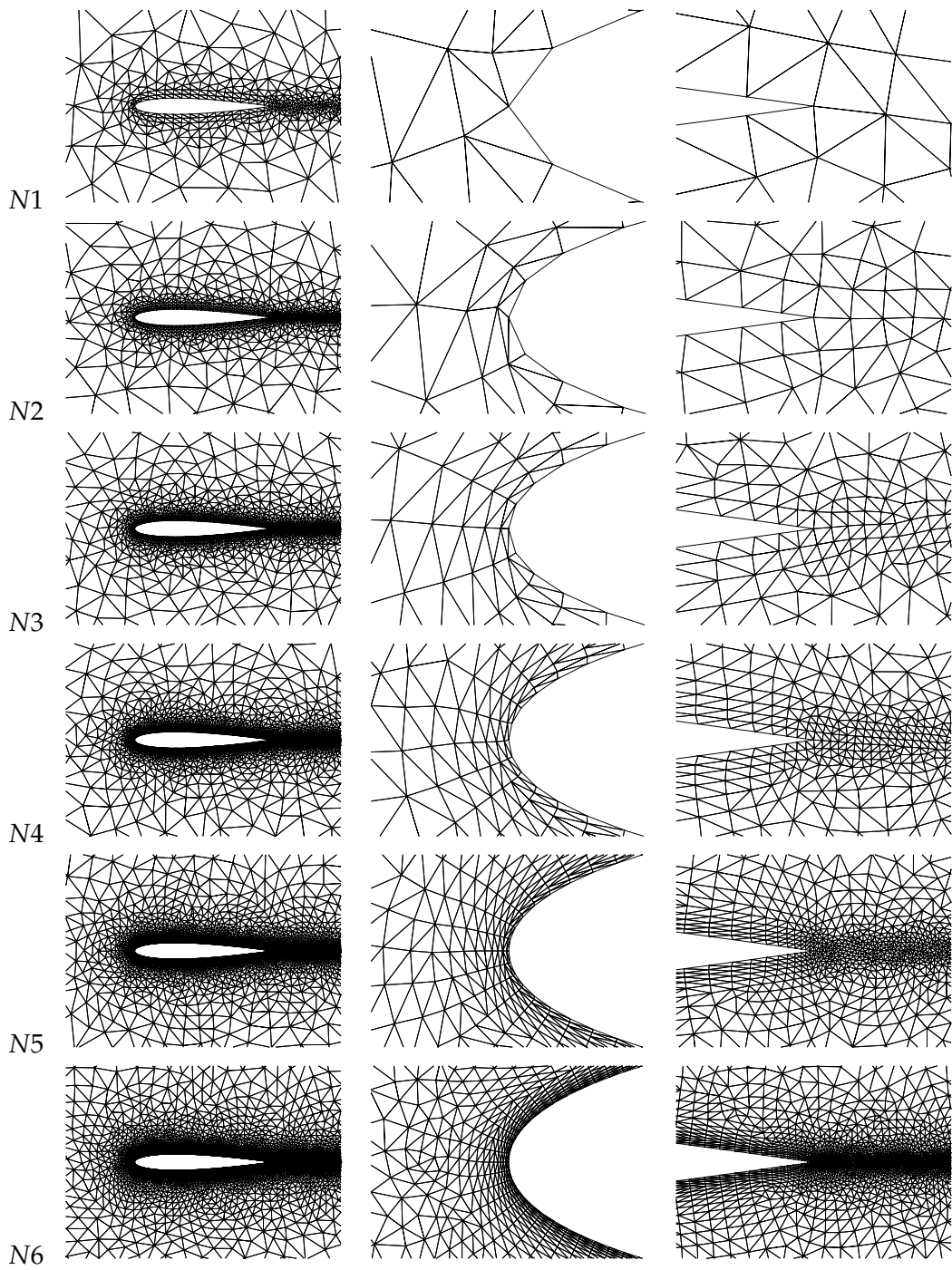
Figure 11: Computational grids $N1 - N6$ around the NACA0012 profile (left) with details around the leading (middle) and trailing edges (right)

mesh	$N1$	$N2$	$N3$	$N4$	$N5$	$N6$
$\#\mathcal{T}_h$	1148	2262	4216	8482	17888	40440
$1/\sqrt{\#\mathcal{T}_h}$	2.95E-02	2.10E-02	1.54E-02	1.09E-02	7.48E-03	4.97E-03

P_k	C_W	$N1$	$N2$	$N3$	$N4$	$N5$	$N6$
P_1	1	0.03322	0.04913	0.05288	0.05429	0.05470	0.05492
P_1	5	0.04289	0.04945	0.05150	0.05356	0.05459	0.05488
P_1	25	0.04692	0.04749	0.04910	0.05203	0.05379	0.05448
P_1	250	0.04157	0.04217	0.04605	0.05093	0.05271	0.05379
P_2	1	0.05538	0.05548	0.05489	0.05482	0.05486	–
P_2	5	0.05431	0.05423	0.05436	0.05467	0.05473	–
P_2	25	0.05167	0.05199	0.05373	0.05458	0.05473	–
P_2	250	0.04796	0.05137	0.05337	0.05428	0.05459	–
P_3	1	0.05939	0.05599	0.05500	0.05492	–	–
P_3	5	0.05783	0.05523	0.05467	0.05468	–	–
P_3	25	0.05475	0.05393	0.05374	0.05471	–	–
P_3	250	0.05178	0.05232	0.05477	0.05480	–	–

Table 3: NACA 0012 profile ($M = 0.5$, $\alpha = 0°$, $Re = 5000$), numbers of elements ($= \#\mathcal{T}_h$) and mesh sizes ($= 1/\sqrt{\#\mathcal{T}_h}$) of grids $N1 - N6$ and the corresponding values of the drag coefficient c_D computed by the NIPG variant of the BDF-DGFE method for different values of C_W

Finally, we carried out additional computations on an adaptively refined grid $A1$ (obtained by the anisotropic adaptation technique [18], [19]) having 2 600 elements, see Figure 13 (top). Table 4 shows a comparison of the pressure ($c_{D,p}$) and viscous parts ($c_{D,v}$) of the drag coefficient (c_D) obtained by P_1, P_2 and P_3 approximations on grid $A1$ with reference values from [48], [6] and our previous results [20]. Figure 14 show the corresponding distributions of the skin friction coefficient in comparison with an "exact" solution obtain by an "overkill" computation. The isolines of the Mach number are shown in Figure 15. We observe an increase of accuracy for increasing polynomial degree of approximation.

6.3   Unsteady flow around NACA0012 profile

The last example represents a flow around the profile NACA 0012 at the free stream Mach number $M = 0.85$, the angle of attack $\alpha = 0°$ and Reynolds number $Re = 10000$. The walls of the profile are adiabatic. This flow regime leads to an unsteady solution and hence a sufficient accuracy with respect to time is required (on the contrary to the previous steady-steady examples).

The computations were carried out on the an adaptively refined grid $A2$ having 3 206 elements, see Figure 13 (bottom). Figure 16 shows a dependence of the drag (c_D) and lift
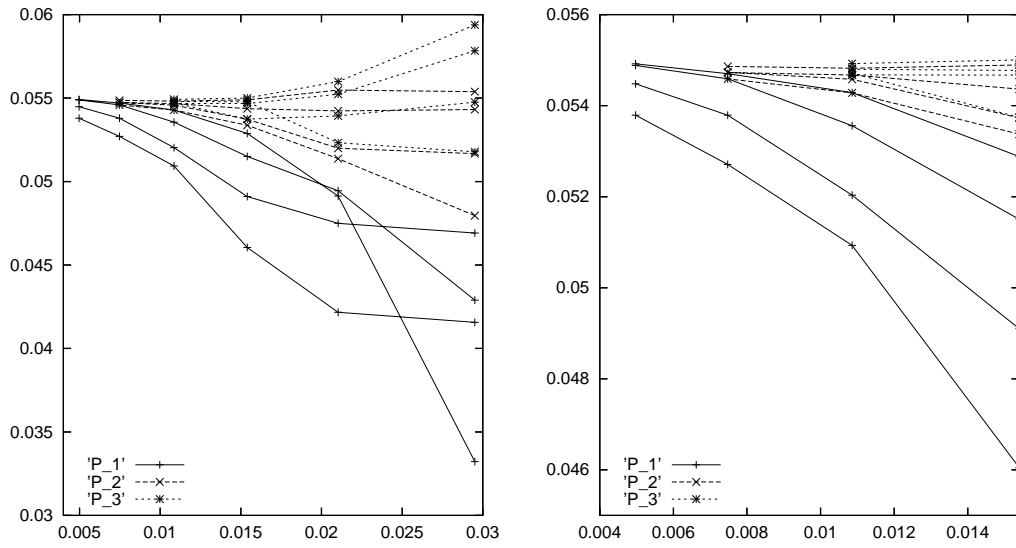
Figure 12: NACA 0012 profile (M=0.5, α=0°, Re=5000), visualization of results from Table 3, the dependencies of the drag coefficient c_D on mesh size ($=1/\sqrt{\#\mathcal{T}_h}$) obtained by the NIPG variant of the BDF-DGFE method for different values of C_W and P_1, P_2 and P_3 approximations on meshes $N1 - N6$ (left) and its detail on meshes $N3 - N6$ (right)
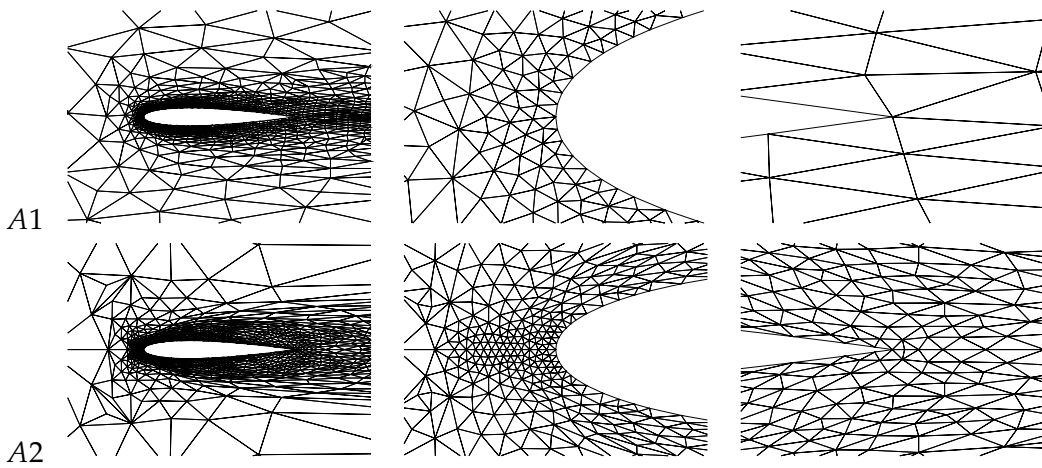

Figure 13: Adaptively refined grids $A1$ and $A2$ around the NACA0012 profile (left) with details around the leading (middle) and trailing edges (right)

method	$\#\mathcal{T}_h$	DOF	$c_{D,p}$	$c_{D,v}$	c_D
BDF-DGM – P_1	2 600	31 200	0.02441	0.02894	0.05335
BDF-DGM – P_2	2 600	62 400	0.02241	0.03173	0.05414
BDF-DGM – P_3	2 600	104 000	0.02279	0.03216	0.05495
[20] – P_1	6 792	81 504	0.02309	0.03113	0.05422
[48] – P_0	32 768	131 072	0.02256	0.03301	0.05557
[48] – P_0	131 072	524 288	0.02235	0.03299	0.05534
[6] – P_1	2 048	24 576	0.01963	0.03051	0.05014
[6] – P_2	2 048	49 152	0.01991	0.03361	0.05352
[6] – P_3	2 048	81 920	0.02208	0.03303	0.05511

Table 4: NACA 0012 profile ($M=0.5$, $\alpha=0°$, $Re=5000$), values of $c_{D,p}$, $c_{D,v}$ and c_D obtained by the BDF-DGFE method on mesh $A1$ in the comparison with our former results [20], finite volume computations from [48] and discontinuous Galerkin solutions obtained by piecewise linear (P_1), quadratic (P_2) and cubic approximations (P_3) in [6]
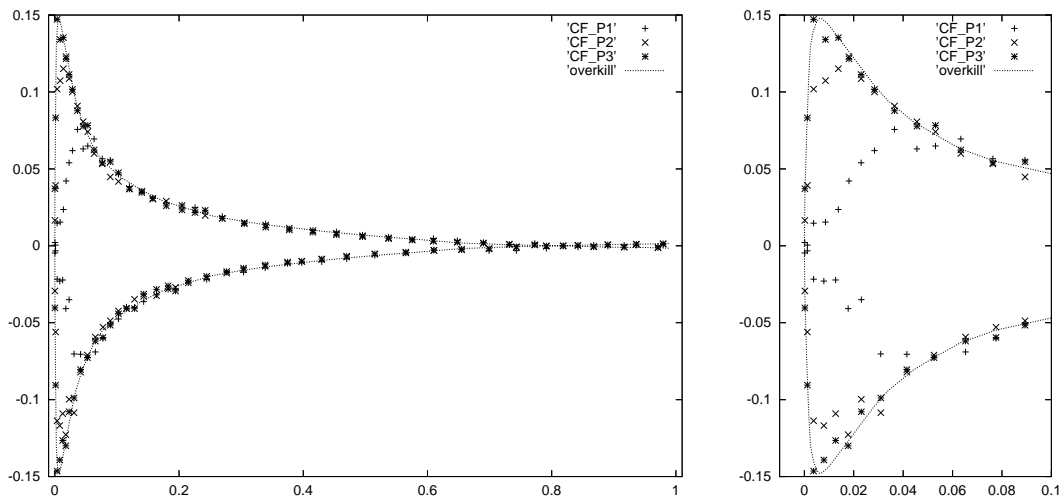
Figure 14: NACA 0012 profile ($M=0.5$, $\alpha=0°$, $Re=5000$), distribution of the skin friction coefficient (left) with a detail around leading edge (right) obtained by piecewise linear (CF_P1), quadratic (CF_P2) and cubic approximations (CF_P3) on mesh $A1$ in comparison with "an exact" solution obtained by an "overkill" computation
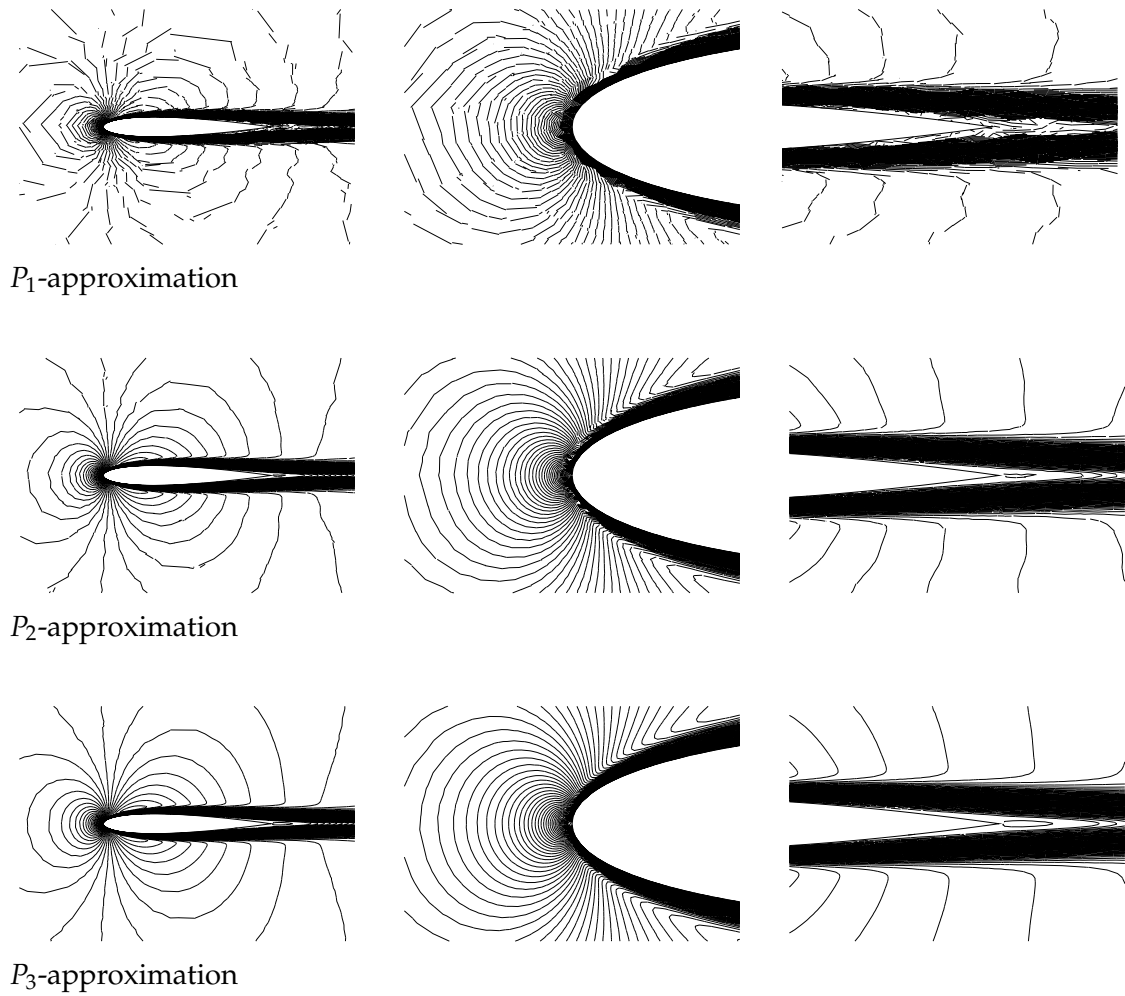
P_1-approximation

P_2-approximation

P_3-approximation

Figure 15: NACA 0012 profile ($M = 0.5$, $\alpha = 0°$, $Re = 5000$), isolines of the Mach number (left) with details around the leading (middle) and trailing edges (right) computed by P_1, P_2 and P_3 approximations

(c_L) coefficients on time obtained by the BDF-DGFE method with piecewise linear (P1), quadratic (P2) and cubic (P3) polynomial approximation in space and the third order in time. A characteristic development of oscillations of c_L are observed, see, e.g., [47]. Moreover, Figure 17 shows a propagation of the lift coefficient obtained with the BDF-DGFE methods with the second and third order accuracy with respect to time in a comparison with reference solution (obtained by an "overkill" computation with respect to time). Figure 18 shows the density distribution at six time instants within one period of the lift coefficient obtained the piecewise cubic polynomial approximation with respect to space and third order of accuracy with respect to time.

7 Conclusion

We carried out a numerical solution of the compressible Navier-Stokes equations by a combination of the discontinuous Galerkin finite element method and the backward difference formulae scheme (BDF-DGFE method). This scheme is sufficiently stable, have a high order of approximation with respect to space and time coordinates and at each time step we solve a linear algebraic problem. Presented numerical examples of steady as well as unsteady flows give promising results.

There are several open problems connected with the use of the BDF-DGFE method to the Navier-Stokes equations:

- an optimization of the method with respect to the computational time, particularly, the choice of the size of time step, type of linear algebra solver and its stopping criterion,

- a use of a hp-adaptation approach based on suitable a posteriori error analysis.

The work in progress is the implementation of the three-dimensional variant of the BDF-DGFE method.

Appendix

The matrices $\boldsymbol{K}_{s,k} \equiv \{K_{s,k}^{(m,n)}\}_{m,n=1}^{d+2}$, $s,k = 1,\ldots,d$ introduced by (2.15) have (for $d=3$) the following form:

$$
\boldsymbol{K}_{1,1} = \begin{pmatrix}
0 & 0 & 0 & 0 & 0 \\
-\frac{4}{3}\frac{w_2}{Re\,w_1^2} & \frac{4}{3}\frac{1}{Re\,w_1} & 0 & 0 & 0 \\
-\frac{w_3}{Re\,w_1^2} & 0 & \frac{1}{Re\,w_1} & 0 & 0 \\
-\frac{w_4}{Re\,w_1^2} & 0 & 0 & \frac{1}{Re\,w_1} & 0 \\
K_{1,1}^{(5,1)} & \frac{1}{Re}\left(\frac{4}{3} - \frac{\gamma}{Pr}\right)\frac{w_2}{w_1^2} & \frac{1}{Re}\left(1 - \frac{\gamma}{Pr}\right)\frac{w_3}{w_1^2} & \frac{1}{Re}\left(1 - \frac{\gamma}{Pr}\right)\frac{w_4}{w_1^2} & \frac{\gamma}{Re\,Pr}\frac{1}{w_1}
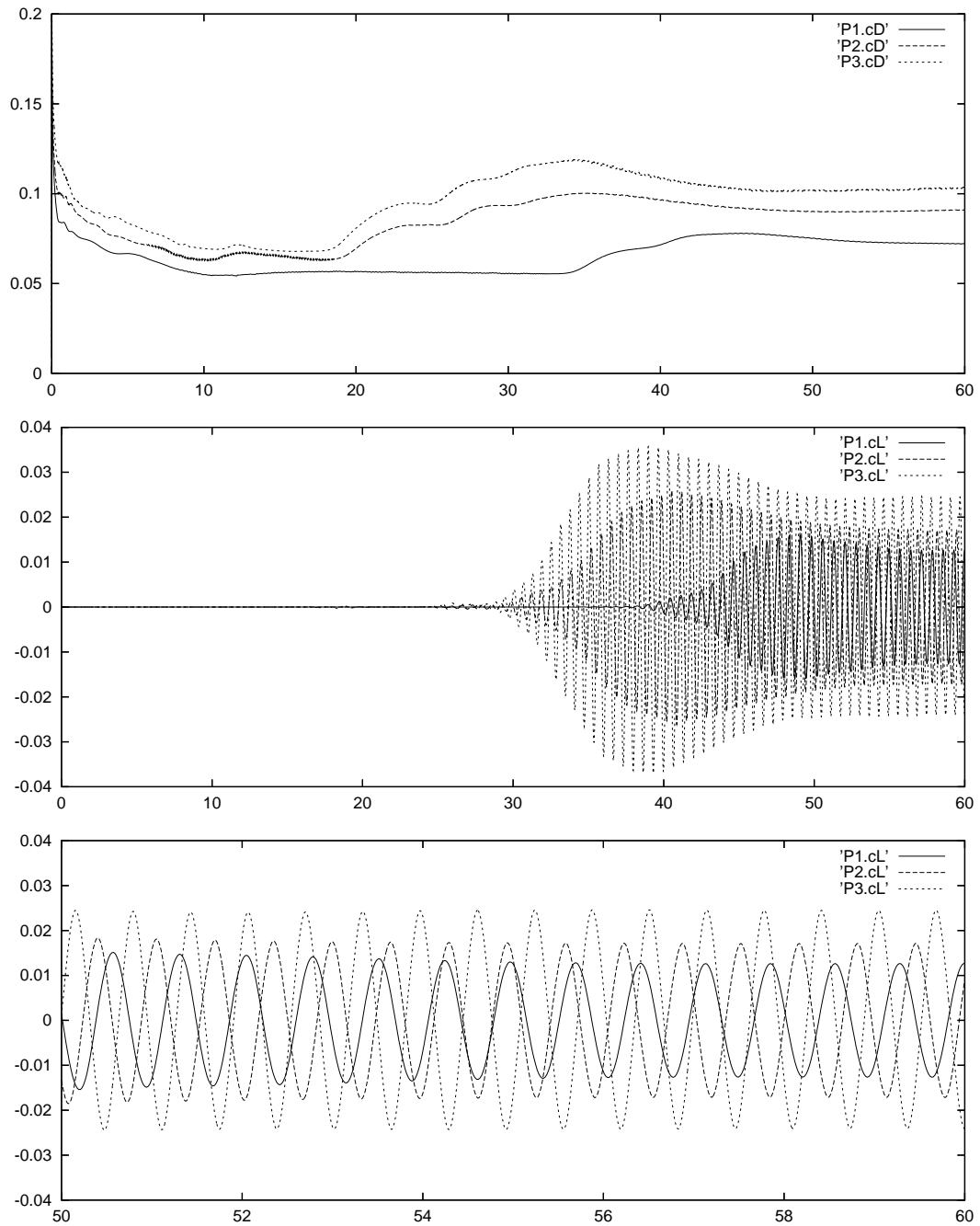\end{pmatrix}, \qquad (7.1)
$$

Figure 16: NACA 0012 profile ($M=0.85$, $\alpha=0°$, $Re=10000$), dependence of the drag (up) and lift (middle and detail down) coefficients on time computed by the BDF-DGFE method with piecewise linear (P1), quadratic (P2) and cubic (P3) approximation in space and third order in time
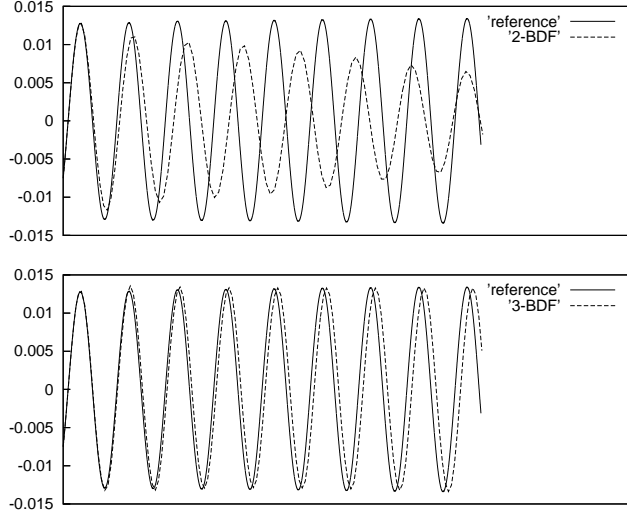
Figure 17: NACA 0012 profile ($M = 0.85$, $\alpha = 0°$, $Re = 10000$), dependence of the lift coefficient on time computed by the BDF-DGFE method with the second (up) and third (down) order of accuracy with respect to time in comparison with the reference solution

with $K_{1,1}^{(5,1)} = -\frac{1}{Re\,w_1^3}\left(\frac{4}{3}w_2^2 + w_3^2 + w_4^2\right) + \frac{\gamma}{Re\,Pr}\left(-\frac{w_5}{w_1^2} + \frac{w_2^2+w_3^2+w_4^2}{w_1^3}\right)$,

$$
\boldsymbol{K}_{2,2} = \begin{pmatrix}
0 & 0 & 0 & 0 & 0 \\
-\frac{w_2}{Re\,w_1^2} & \frac{1}{Re\,w_1} & 0 & 0 & 0 \\
-\frac{4}{3}\frac{w_3}{Re\,w_1^2} & 0 & \frac{4}{3}\frac{1}{Re\,w_1} & 0 & 0 \\
-\frac{w_4}{Re\,w_1^2} & 0 & 0 & \frac{1}{Re\,w_1} & 0 \\
K_{2,2}^{(5,1)} & \frac{1}{Re}\left(1-\frac{\gamma}{Pr}\right)\frac{w_2}{w_1^2} & \frac{1}{Re}\left(\frac{4}{3}-\frac{\gamma}{Pr}\right)\frac{w_3}{w_1^2} & \frac{1}{Re}\left(1-\frac{\gamma}{Pr}\right)\frac{w_4}{w_1^2} & \frac{\gamma}{Re\,Pr}\frac{1}{w_1}
\end{pmatrix},
\qquad (7.2)
$$

with $K_{2,2}^{(5,1)} = -\frac{1}{Re\,w_1^3}\left(w_2^2 + \frac{4}{3}w_3^2 + w_4^2\right) + \frac{\gamma}{Re\,Pr}\left(-\frac{w_5}{w_1^2} + \frac{w_2^2+w_3^2+w_4^2}{w_1^3}\right)$,

$$
\boldsymbol{K}_{3,3} = \begin{pmatrix}
0 & 0 & 0 & 0 & 0 \\
-\frac{w_2}{Re\,w_1^2} & \frac{1}{Re\,w_1} & 0 & 0 & 0 \\
-\frac{w_3}{Re\,w_1^2} & 0 & \frac{1}{Re\,w_1} & 0 & 0 \\
-\frac{4}{3}\frac{w_4}{Re\,w_1^2} & 0 & 0 & \frac{4}{3}\frac{1}{Re\,w_1} & 0 \\
K_{3,3}^{(5,1)} & \frac{1}{Re}\left(1-\frac{\gamma}{Pr}\right)\frac{w_2}{w_1^2} & \frac{1}{Re}\left(1-\frac{\gamma}{Pr}\right)\frac{w_3}{w_1^2} & \frac{1}{Re}\left(\frac{4}{3}-\frac{\gamma}{Pr}\right)\frac{w_4}{w_1^2} & \frac{\gamma}{Re\,Pr}\frac{1}{w_1}
\end{pmatrix},
\qquad (7.3)
$$

with $K_{3,3}^{(5,1)} = -\frac{1}{Re\,w_1^3}\left(w_2^2 + w_3^2 + \frac{4}{3}w_4^2\right) + \frac{\gamma}{Re\,Pr}\left(-\frac{w_5}{w_1^2} + \frac{w_2^2+w_3^2+w_4^2}{w_1^3}\right)$,
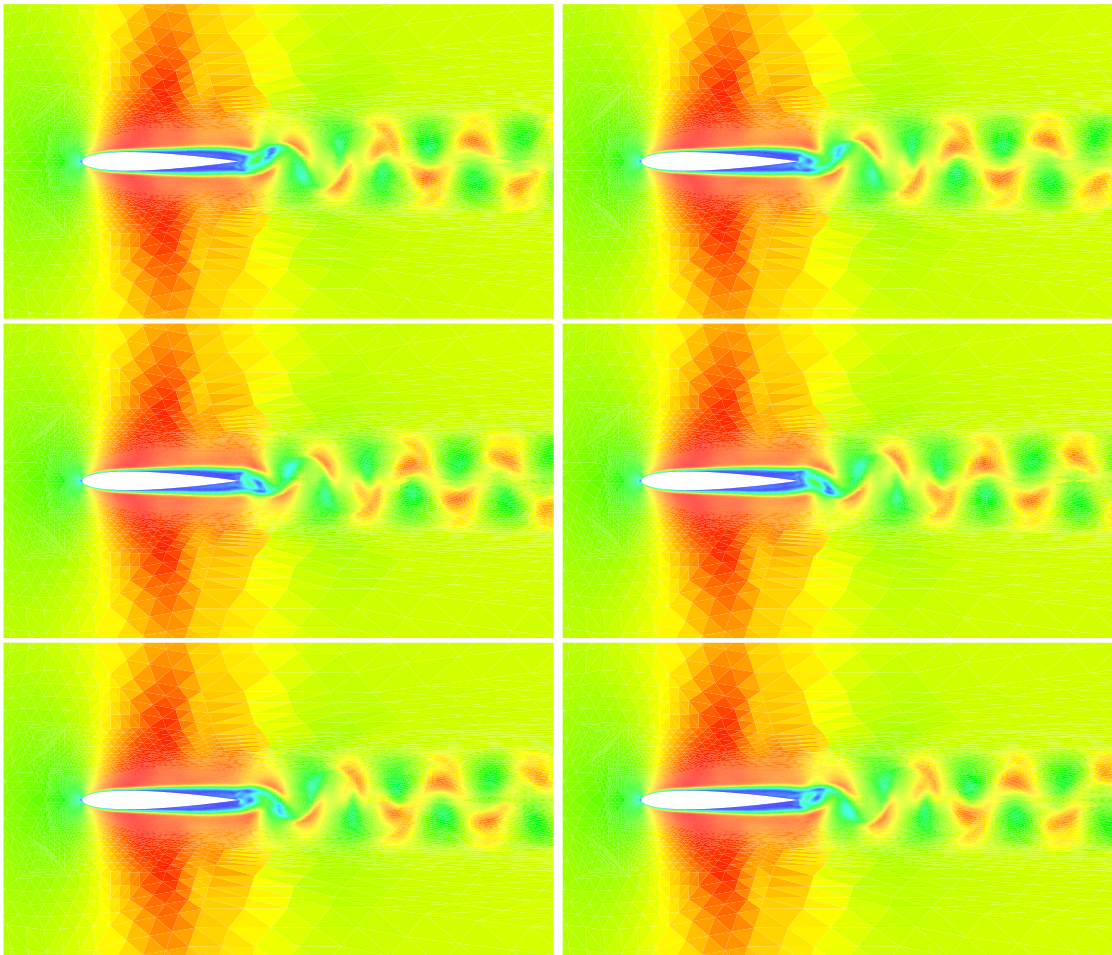
Figure 18: NACA 0012 profile ($M=0.85$, $\alpha=0°$, $Re=10000$), P_3-approximation in space, third order in time, Mach number distribution at 6 time instants within one period of the lift coefficient oscillations

$$\boldsymbol{K}_{1,2}=\begin{pmatrix} 0 & 0 & 0 & 0 & 0 \\ \frac{2}{3}\frac{w_3}{Re\,w_1^2} & 0 & -\frac{2}{3}\frac{1}{Re\,w_1} & 0 & 0 \\ -\frac{w_2}{Re\,w_1^2} & \frac{1}{Re\,w_1} & 0 & 0 & 0 \\ 0 & 0 & 0 & 0 & 0 \\ -\frac{1}{3}\frac{w_2 w_3}{Re\,w_1^3} & \frac{w_3}{Re\,w_1^2} & -\frac{2}{3}\frac{w_2}{Re\,w_1^2} & 0 & 0 \end{pmatrix}, \quad \boldsymbol{K}_{1,3}=\begin{pmatrix} 0 & 0 & 0 & 0 & 0 \\ \frac{2}{3}\frac{w_4}{Re\,w_1^2} & 0 & 0 & -\frac{2}{3}\frac{1}{Re\,w_1} & 0 \\ 0 & 0 & 0 & 0 & 0 \\ -\frac{w_2}{Re\,w_1^2} & \frac{1}{Re\,w_1} & 0 & 0 & 0 \\ -\frac{1}{3}\frac{w_2 w_4}{Re\,w_1^3} & \frac{w_4}{Re\,w_1^2} & 0 & -\frac{2}{3}\frac{w_2}{Re\,w_1^2} & 0 \end{pmatrix},$$

$$\tag{7.4}$$

$$\boldsymbol{K}_{2,1}=\begin{pmatrix} 0 & 0 & 0 & 0 & 0 \\ -\frac{w_3}{Re\,w_1^2} & 0 & \frac{1}{Re\,w_1} & 0 & 0 \\ \frac{2}{3}\frac{w_2}{Re\,w_1^2} & -\frac{2}{3}\frac{1}{Re\,w_1} & 0 & 0 & 0 \\ 0 & 0 & 0 & 0 & 0 \\ -\frac{1}{3}\frac{w_2 w_3}{Re\,w_1^3} & -\frac{2}{3}\frac{w_3}{Re\,w_1^2} & \frac{w_2}{Re\,w_1^2} & 0 & 0 \end{pmatrix}, \quad \boldsymbol{K}_{2,3}=\begin{pmatrix} 0 & 0 & 0 & 0 & 0 \\ 0 & 0 & 0 & 0 & 0 \\ \frac{2}{3}\frac{w_4}{Re\,w_1^2} & 0 & 0 & -\frac{2}{3}\frac{1}{Re\,w_1} & 0 \\ -\frac{w_3}{Re\,w_1^2} & 0 & \frac{1}{Re\,w_1} & 0 & 0 \\ -\frac{1}{3}\frac{w_3 w_4}{Re\,w_1^3} & 0 & \frac{w_4}{Re\,w_1^2} & -\frac{2}{3}\frac{w_2}{Re\,w_1^2} & 0 \end{pmatrix},$$

$$\tag{7.5}$$

$$\boldsymbol{K}_{3,1}=\begin{pmatrix} 0 & 0 & 0 & 0 & 0 \\ -\frac{w_4}{Re\,w_1^2} & 0 & 0 & \frac{1}{Re\,w_1} & 0 \\ 0 & 0 & 0 & 0 & 0 \\ \frac{2}{3}\frac{w_2}{Re\,w_1^2} & -\frac{2}{3}\frac{1}{Re\,w_1} & 0 & 0 & 0 \\ -\frac{1}{3}\frac{w_2 w_4}{Re\,w_1^3} & -\frac{2}{3}\frac{w_4}{Re\,w_1^2} & 0 & \frac{w_2}{Re\,w_1^2} & 0 \end{pmatrix}, \quad \boldsymbol{K}_{3,2}=\begin{pmatrix} 0 & 0 & 0 & 0 & 0 \\ 0 & 0 & 0 & 0 & 0 \\ -\frac{w_4}{Re\,w_1^2} & 0 & 0 & \frac{1}{Re\,w_1} & 0 \\ \frac{2}{3}\frac{w_3}{Re\,w_1^2} & 0 & -\frac{2}{3}\frac{1}{Re\,w_1} & 0 & 0 \\ -\frac{1}{3}\frac{w_3 w_4}{Re\,w_1^3} & 0 & -\frac{2}{3}\frac{w_4}{Re\,w_1^2} & \frac{w_3}{Re\,w_1^2} & 0 \end{pmatrix}.$$

$$\tag{7.6}$$

For $d=2$, the form of $\boldsymbol{K}_{s,k}$, $s,k=1,2$ can be easily derived from (7.1) – (7.6 by removing fourth rows and columns of matrices $\boldsymbol{K}_{s,k}$, symbolically putting $w_4:=0$ and finally "renaming" w_5 by w_4. See also, e.g., [35, Section 4.3] or [39] where the explicit forms of $\boldsymbol{K}_{s,k}$, $s,k=1,2$ for $d=2$ are given.

The matrices $\boldsymbol{D}_{s,k}\equiv\left\{D_{s,k}^{(m,n)}\right\}_{m,n=1}^{d+2}$, $k=0,1,\dots,d$, $s=1,\dots,d$ introduced by (2.21) are given by

$$\boldsymbol{D}_{1,0}(\boldsymbol{w},\nabla\boldsymbol{w})\equiv\begin{pmatrix} 0 & 0 & 0 & 0 & 0 \\ 0 & -\frac{4}{3}\frac{1}{Re\,w_1^2}\frac{\partial w_1}{\partial x_1} & \frac{2}{3}\frac{1}{Re\,w_1^2}\frac{\partial w_1}{\partial x_2} & \frac{2}{3}\frac{1}{Re\,w_1^2}\frac{\partial w_1}{\partial x_3} & 0 \\ 0 & -\frac{1}{Re\,w_1^2}\frac{\partial w_1}{\partial x_2} & -\frac{1}{Re\,w_1^2}\frac{\partial w_1}{\partial x_1} & 0 & 0 \\ 0 & -\frac{1}{Re\,w_1^2}\frac{\partial w_1}{\partial x_3} & 0 & -\frac{1}{Re\,w_1^2}\frac{\partial w_1}{\partial x_1} & 0 \\ 0 & D_{1,0}^{(5,2)} & D_{1,0}^{(5,3)} & D_{1,0}^{(5,4)} & -\frac{\gamma}{Pr}\frac{1}{Re\,w_1^2}\frac{\partial w_1}{\partial x_1} \end{pmatrix} \tag{7.7}$$

with

$$D_{1,0}^{(5,2)} \equiv -\frac{1}{Rew_1^3}\left(\frac{4}{3}w_2\frac{\partial w_1}{\partial x_1}+w_3\frac{\partial w_1}{\partial x_2}+w_4\frac{\partial w_1}{\partial x_3}\right)+\frac{\gamma}{Pr}\frac{1}{Rew_1^2}\frac{w_2}{w_1}\frac{\partial w_1}{\partial x_1},$$

$$D_{1,0}^{(5,3)} \equiv \frac{1}{Rew_1^3}\left(\frac{2}{3}w_2\frac{\partial w_1}{\partial x_2}-w_3\frac{\partial w_1}{\partial x_1}\right)+\frac{\gamma}{Pr}\frac{1}{Rew_1^2}\frac{w_3}{w_1}\frac{\partial w_1}{\partial x_1},$$

$$D_{1,0}^{(5,4)} \equiv \frac{1}{Rew_1^3}\left(\frac{2}{3}w_2\frac{\partial w_1}{\partial x_3}-w_4\frac{\partial w_1}{\partial x_1}\right)+\frac{\gamma}{Pr}\frac{1}{Rew_1^2}\frac{w_4}{w_1}\frac{\partial w_1}{\partial x_1},$$

$$\boldsymbol{D}_{2,0}(\boldsymbol{w},\nabla\boldsymbol{w}) \equiv \begin{pmatrix} 0 & 0 & 0 & 0 & 0 \\ 0 & -\frac{1}{Rew_1^2}\frac{\partial w_1}{\partial x_2} & -\frac{1}{Rew_1^2}\frac{\partial w_1}{\partial x_1} & 0 & 0 \\ 0 & \frac{2}{3}\frac{1}{Rew_1^2}\frac{\partial w_1}{\partial x_1} & -\frac{4}{3}\frac{1}{Rew_1^2}\frac{\partial w_1}{\partial x_2} & \frac{2}{3}\frac{1}{Rew_1^2}\frac{\partial w_1}{\partial x_3} & 0 \\ 0 & 0 & -\frac{1}{Rew_1^2}\frac{\partial w_1}{\partial x_3} & -\frac{1}{Rew_1^2}\frac{\partial w_1}{\partial x_2} & 0 \\ 0 & D_{2,0}^{(5,2)} & D_{2,0}^{(5,3)} & D_{2,0}^{(5,4)} & -\frac{\gamma}{Pr}\frac{1}{Rew_1^2}\frac{\partial w_1}{\partial x_2} \end{pmatrix} \tag{7.8}$$

with

$$D_{2,0}^{(5,2)} \equiv \frac{1}{Rew_1^3}\left(\frac{2}{3}w_3\frac{\partial w_1}{\partial x_1}-w_3\frac{\partial w_1}{\partial x_2}\right)+\frac{\gamma}{Pr}\frac{1}{Rew_1^2}\frac{w_2}{w_1}\frac{\partial w_1}{\partial x_2},$$

$$D_{2,0}^{(5,3)} \equiv -\frac{1}{Rew_1^3}\left(w_2\frac{\partial w_1}{\partial x_1}+\frac{4}{3}w_3\frac{\partial w_1}{\partial x_2}+w_4\frac{\partial w_1}{\partial x_3}\right)+\frac{\gamma}{Pr}\frac{1}{Rew_1^2}\frac{w_3}{w_1}\frac{\partial w_1}{\partial x_2},$$

$$D_{2,0}^{(5,4)} \equiv \frac{1}{Rew_1^3}\left(\frac{2}{3}w_3\frac{\partial w_1}{\partial x_3}-w_4\frac{\partial w_1}{\partial x_2}\right)+\frac{\gamma}{Pr}\frac{1}{Rew_1^2}\frac{w_4}{w_1}\frac{\partial w_1}{\partial x_3},$$

$$\boldsymbol{D}_{3,0}(\boldsymbol{w},\nabla\boldsymbol{w}) \equiv \begin{pmatrix} 0 & 0 & 0 & 0 & 0 \\ 0 & -\frac{1}{Rew_1^2}\frac{\partial w_1}{\partial x_3} & 0 & -\frac{1}{Rew_1^2}\frac{\partial w_1}{\partial x_1} & 0 \\ 0 & 0 & -\frac{1}{Rew_1^2}\frac{\partial w_1}{\partial x_3} & -\frac{1}{Rew_1^2}\frac{\partial w_1}{\partial x_2} & 0 \\ 0 & \frac{2}{3}\frac{1}{Rew_1^2}\frac{\partial w_1}{\partial x_1} & \frac{2}{3}\frac{1}{Rew_1^2}\frac{\partial w_1}{\partial x_2} & -\frac{4}{3}\frac{1}{Rew_1^2}\frac{\partial w_1}{\partial x_3} & 0 \\ 0 & D_{3,0}^{(5,2)} & D_{3,0}^{(5,3)} & D_{3,0}^{(5,4)} & -\frac{\gamma}{Pr}\frac{1}{Rew_1^2}\frac{\partial w_1}{\partial x_3} \end{pmatrix} \tag{7.9}$$

with

$$D_{3,0}^{(5,2)} \equiv \frac{1}{Rew_1^3}\left(\frac{2}{3}w_4\frac{\partial w_1}{\partial x_1}-w_2\frac{\partial w_1}{\partial x_3}\right)+\frac{\gamma}{Pr}\frac{1}{Rew_1^2}\frac{w_2}{w_1}\frac{\partial w_1}{\partial x_2},$$

$$D_{3,0}^{(5,3)} \equiv \frac{1}{Rew_1^3}\left(\frac{2}{3}w_4\frac{\partial w_1}{\partial x_2}-w_3\frac{\partial w_1}{\partial x_3}\right)+\frac{\gamma}{Pr}\frac{1}{Rew_1^2}\frac{w_3}{w_1}\frac{\partial w_1}{\partial x_2},$$

$$D_{3,0}^{(5,4)} \equiv -\frac{1}{Rew_1^3}\left(w_2\frac{\partial w_1}{\partial x_1}+w_3\frac{\partial w_1}{\partial x_2}+\frac{4}{3}w_4\frac{\partial w_1}{\partial x_3}\right)+\frac{\gamma}{Pr}\frac{1}{Rew_1^2}\frac{w_4}{w_1}\frac{\partial w_1}{\partial x_3}.$$

For $d=2$, the form of $\boldsymbol{D}_{s,0}$, $s=1,2$ can be easily derived from (7.7) – (7.9 by removing fourth rows and columns of matrices $\boldsymbol{D}_{s,0}$, symbolically putting $w_4:=0$ and finally "renaming" w_5 by w_4.

The matrix elements of $\boldsymbol{D}_{s,k}$, $s,k=1,\ldots,d$ are defined by

$$D_{s,k}^{(m,n)} = \begin{cases} K_{s,k}^{(m,n)} & \text{for } n=2,\ldots,d+2 \\ 0 & \text{for } n=1 \end{cases} , \quad m=1,\ldots,d+2, \ s,k=1,\ldots,d, \qquad (7.10)$$

where $K_{s,k}^{(m,n)}$ $m,n=1,\ldots,d+2$ are elements of matrices $\boldsymbol{K}_{s,k}$, $s,k=1,\ldots,d$ given by (7.1) – (7.6).

Acknowledgments

References

[1] ADIGMA. Adaptive higher-order variational methods for aerodynamic applications in industry, Specific Targeted Research Project no. 30719 supported by European Ccommison. URL: http://www.dlr.de/as/en/Desktopdefault.aspx/tabid-2035/2979_read-4582/.

[2] D. N. Arnold. An interior penalty finite element method with discontinuous elements. *SIAM J. Numer. Anal.*, 19(4):742–760, 1982.

[3] D. N. Arnold, F. Brezzi, B. Cockburn, and L. D. Marini. Unified analysis of discontinuous Galerkin methods for elliptic problems. *SIAM J. Numer. Anal.*, 39(5):1749–1779, 2002.

[4] I. Babuška, C. E. Baumann, and J. T. Oden. A discontinuous *hp* finite element method for diffusion problems: 1-d analysis. *Computers and Mathematics with Applications*, 37:103–122, 1999.

[5] F. Bassi, A. Crivellini, S. Rebay, and M. Savini. Discontinuous Galerkin solution of the Reynolds averaged Navier-Stokes and *k-ω* turbulence model equations. *Comput. Fluids*, 34:507–540, 2005.

[6] F. Bassi and S. Rebay. A high-order accurate discontinuous finite element method for the numerical solution of the compressible Navier–Stokes equations. *J. Comput. Phys.*, 131:267–279, 1997.

[7] F. Bassi and S. Rebay. High-order accurate discontinuous finite element solution of the 2D Euler equations. *J. Comput. Phys.*, 138:251–285, 1997.

[8] F. Bassi and S. Rebay. A high order discontinuous Galerkin method for compressible turbulent flow. In B. Cockburn, G. E. Karniadakis, and C.-W. Shu, editors, *Discontinuous Galerkin*

Method: Theory, Computations and Applications, Lecture Notes in Computational Science and Engineering 11, pages 113–123. Springer-Verlag, 2000.

[9] F. Bassi and S. Rebay. Numerical evaluation of two discontinuous Galerkin methods for the compressible Navier–Stokes equations. *Int. J. Numer. Methods Fluids*, 40:197–207, 2002.

[10] C. E. Baumann and J. T. Oden. A discontinuous hp finite element method for the Euler and Navier-Stokes equations. *Int. J. Numer. Methods Fluids*, 31(1):79–95, 1999.

[11] P. Birken, J. D. Tebbens, A. Meister, and M. Tůma. Preconditioner updates applied to CFD model problems. Mathematische schriften kassel preprint-reihe fachbereich mathematik/informatik, Universität Kassel, 2007.

[12] P. G. Ciarlet. *The Finite Elements Method for Elliptic Problems*. North-Holland, Amsterdam, New York, Oxford, 1979.

[13] B. Cockburn. Discontinuous Galerkin methods for convection dominated problems. In T. J. Barth and H. Deconinck, editors, *High–Order Methods for Computational Physics*, Lecture Notes in Computational Science and Engineering 9, pages 69–224. Springer, Berlin, 1999.

[14] B. Cockburn, S. Hou, and C. W. Shu. TVB Runge-Kutta local projection discontinuous Galerkin finite element for conservation laws IV: The multi-dimensional case. *Math. Comp.*, 54:545–581, 1990.

[15] B. Cockburn, G. E. Karniadakis, and C.-W. Shu, editors. *Discontinuous Galerkin Methods*. Springer, Berlin, 2000.

[16] M. Crouzeix. Une méthode multipas implicit-explicit pour l'approximation des équations d'évolutions paraboliques. *Numer. Math.*, 35:27–276, 1980.

[17] C. N. Dawson, S. Sun, and M. F. Wheeler. Compatible algorithms for coupled flow and transport. *Comput. Meth. Appl. Mech. Engng.*, 193:2565–2580., 2004.

[18] V. Dolejší. Anisotropic mesh adaptation for finite volume and finite element methods on triangular meshes. *Comput. Vis. Sci.*, 1(3):165–178, 1998.

[19] V. Dolejší. Anisotropic mesh adaptation technique for viscous flow simulation. *East-West J. Numer. Math.*, 9(1):1–24, 2001.

[20] V. Dolejší. On the discontinuous Galerkin method for the numerical solution of the Navier–Stokes equations. *Int. J. Numer. Methods Fluids*, 45:1083–1106, 2004.

[21] V. Dolejší. An efficient implementation of the semi-implicit discontinuous galerkin method for compressible flow simulation. In T. Vejchodský J. Chleboun, K. Segeth, editor, *Programs and Algorithms of Numerical Mathematics 13*, pages 74–79. Programs and Algorithms of Numerical Mathematics 13, Academy of Science of the Czech Republic, Prague, 2006.

[22] V. Dolejší. Analysis and application of IIPG method to quasilinear nonstationary convection-diffusion problems. *J. Comp. Appl. Math.*, in press.

[23] V. Dolejší and M. Feistauer. On the discontinuous Galerkin method for the numerical solution of compressible high-speed flow. In F. Brezzi, A. Buffa, S. Corsaro, and A. Murli, editors, *Numerical Mathematics and Advanced Applications, ENUMATH 2001*, pages 65–84. Springer-Verlag, Italia, Milano, 2003.

[24] V. Dolejší and M. Feistauer. Error estimates of the discontinuous Galerkin method for nonlinear nonstationary convection-diffusion problems. *Numer. Funct. Anal. Optim.*, 26(25-26):2709–2733, 2005.

[25] V. Dolejší, M. Feistauer, and J. Hozman. Analysis of semi-implicit DGFEM for nonlinear convection-diffusion problems. *Comput. Methods Appl. Mech. Engrg.*, 196:2813–2827, 2007.

[26] V. Dolejší, M. Feistauer, V. Kučera, and V. Sobotíková. An optimal $L^\infty(L^2)$-error estimate of the discontinuous galerkin method for a nonlinear nonstationary convection-diffusion problem. *IMA J. Numer. Anal.*, in press.

[27] V. Dolejší, M. Feistauer, and V. Sobotíková. A discontinuous Galerkin method for nonlinear convection–diffusion problems. *Comput. Methods Appl. Mech. Engrg.*, 194:2709–2733, 2005.

[28] V. Dolejší and P. Kůs. Adaptive backward difference formula – discontinuous Galerkin finite element method for the solution of conservation laws. *Int. J. Numer. Methods Eng.*, 2007 (published online).

[29] V. Dolejší and M. Vlasák. Analysis of a BDF – DGFE scheme for nonlinear convection-diffusion problems. *Numer. Math.*, 2007 (submitted). Preprint No. MATH-knm-2007/4, Charles University Prague, School of Mathematics, 2007, www.karlin.mff.cuni.cz/ms-preprints.

[30] V. Dolejší. Discontinuous Galerkin method for the numerical simulation of unsteady compressible flow. *WSEAS Transactions on Systems*, 5(5):1083–1090, 2006.

[31] V. Dolejší and M. Feistauer. Semi-implicit discontinuous Galerkin finite element method for the numerical solution of inviscid compressible flow. *J. Comput. Phys.*, 198(2):727–746, 2004.

[32] M. Dumbser and C.-D. Munz. Building blocks for arbitrary high-order discontinuous Galerkin methods. *J. Sci. Comput.*, 27:215–230, 2006.

[33] M. Feistauer. *Mathematical Methods in Fluid Dynamics*. Longman Scientific & Technical, Harlow, 1993.

[34] M. Feistauer, J. Felcman, M. Lukáčová-Medvidová, and G. Warnecke. Error estimates of a combined finite volume – finite element method for nonlinear convection – diffusion problems. *SIAM J. Numer. Anal.*, 36(5):1528–1548, 1999.

[35] M. Feistauer, J. Felcman, and I. Straškraba. *Mathematical and Computational Methods for Compressible Flow*. Oxford University Press, Oxford, 2003.

[36] E. Hairer, S. P. Norsett, and G. Wanner. *Solving ordinary differential equations I, Nonstiff problems*. Number 8 in Springer Series in Computational Mathematics. Springer Verlag, 2000.

[37] R. Hartmann. Adaptive discontinuous galerkin methods with shock-capturing for the compressible navier-stokes equations. *Int. J. Numer. Meth. Fluids*, 51:1131–1156, 2006.

[38] R. Hartmann and P. Houston. Adaptive discontinuous Galerkin finite element methods for the compressible Euler equations. *J. Comput. Phys.*, 183(2):508–532, 2002.

[39] R. Hartmann and P. Houston. Symmetric interior penalty DG methods for the compressible Navier-Stokes equations I: Method formulation. *Int. J. Numer. Anal. Model.*, 1:1–20, 2006.

[40] R. Hartmann and P. Houston. Symmetric interior penalty DG methods for the compressible Navier-Stokes equations II: Goal-oriented a posteriori error estimation. *Int. J. Numer. Anal. Model.*, 3:141–162, 2006.

[41] P. Houston, J. Robson, and E. Süli. Discontinuous Galerkin finite element approximation of quasilinear elliptic boundary value problems I: The scalar case. *IMA J. Numer. Anal.*, 25:726–749, 2005.

[42] P. Houston, C. Schwab, and E. Süli. Discontinuous hp-finite element methods for advection-diffusion problems. *SIAM J. Numer. Anal.*, 39(6):2133–2163, 2002.

[43] C. M. Klaij, J.J.W. van der Vegt, and H. Van der Ven. Pseudo-time stepping for space-time discontinuous Galerkin discretizations of the compressible Navier-Stokes equations. *J. Comput. Phys.*, 219(2):622–643, 2006.

[44] C. M. Klaij, J.J.W. van der Vegt, and H. Van der Ven. Space-time discontinuous Galerkin method for the compressible Navier-Stokes equations. *J. Comput. Phys.*, 217(2):589–611, 2006.

[45] I. Lomtev, C. B.Quillen, and G. E. Karniadakis. Spectral/hp methods for viscous compressible flows on unstructured 2d meshes. *J. Comput. Phys.*, 144(2):325–357, 1998.

[46] F. Lörcher, G. Gassner, and C.-D. Munz. A discontinuous Galerkin scheme based on a spacetime expansion. I. Inviscid compressible flow in one space dimension. *J. Sci. Comput.*,

32(2):175–199, 2007.

[47] S. Mittal. Finite element computation of unsteady viscous compressible flows. *Comput. Methods Appl. Mech. Eng.*, 157:151–175, 1998.

[48] R. Radespiel and R. C. Swanson. An investigation of cell centered and cell vertex multigrid schemes for the Navier-Stokes equations. AIAA paper No. 89-0453, 1989.

[49] B. Rivière and M. F. Wheeler. A discontinuous Galerkin method applied to nonlinear parabolic equations. In B. Cockburn, G. E. Karniadakis, and C.-W. Schu, editors, *Discontinuous Galerkin methods. Theory, computation and applications.*, volume 11 of *Lect. Notes Comput. Sci. Eng.*, pages 231–244. Berlin, Springer, 2000.

[50] B. Rivière, M. F. Wheeler, and V. Girault. Improved energy estimates for interior penalty, constrained and discontinuous Galerkin methods for elliptic problems. I. *Comput. Geosci.*, 3(3-4):337–360, 1999.

[51] B. Rivière, M. F. Wheeler, and V. Girault. A priori error estimates for finite element methods based on discontinuous approximation spaces for elliptic problems. *SIAM J. Numer. Anal.*, 39(3):902–931, 2001.

[52] P. L. Roe. Approximate Riemann solvers, parameter vectors, and difference schemes. *J. Comput. Phys.*, 43(2):357–372, 1981.

[53] S. Sun. *Discontinuous Galerkin methods for reactive transport in porous media*. PhD thesis, The University of Texas, Austin, 2003.

[54] S. Sun and M. F. Wheeler. Symmetric and nonsymmetric discontinuous Galerkin methods for reactive transport in porous media. *SIAM J. Numer. Anal.*, 43(1):195–219, 2005.

[55] R. Temam. *Navier–Stokes Equations. Theory and numerical analysis*. North–Holland, Amsterdam–New York–Oxford, 1977.

[56] J. J. W. van der Vegt and H. van der Ven. Space-time discontinuous Galerkin finite element method with dynamic grid motion for inviscid compressible flows. I: General formulation. *J. Comput. Phys.*, 182(2):546–585, 2002.

[57] H. van der Ven and J. J. W. van der Vegt. Space-time discontinuous Galerkin finite element method with dynamic grid motion for inviscid compressible flows II. efficient flux quadrature. *Comput. Methods Appl. Mech. Engrg.*, 191:4747–4780, 2002.

[58] J. M. Varah. Stability restrictions on second order, three level finite difference scheme for parabolic equations. *SIAM J. Numer. Anal.*, 17(2):300–309, 1980.

[59] G. Vijayasundaram. Transonic flow simulation using upstream centered scheme of Godunov type in finite elements. *J. Comput. Phys.*, 63:416–433, 1986.

[60] P. Wesseling. *Principles of Computational Fluid Dynamics*. Springer, Berlin, 2001.